Copyright
by
Nicole Helbig
1999

MULTI-PASS AMPLIFICATION WITH A BROAD-AREA DIODE LASER

by

NICOLE HELBIG

THESIS

Presented to the Faculty of the Graduate School of

The University of Texas at Austin

in Partial Fulfillment

of the Requirements

for the Degree of

MASTER OF ARTS

THE UNIVERSITY OF TEXAS AT AUSTIN

August 1999

MULTI-PASS AMPLIFICATION WITH A BROAD-AREA DIODE LASER

APPROVED BY
SUPERVISING COMMITTEE:

Supervisor: _____

_____

For Mom.

Acknowledgments

I have had the very good fortune to work in Mark Raizen's Atom Optics Laboratory during my year at the University of Texas at Austin. Mark is not only an endless source for new ideas but also has the ability of creating a nice atmosphere in his lab that makes it fun to work there. Another reason that I enjoyed the year in the lab are the people working there.

Alexander Mück who worked with me on this project through all the up and downs. Thanks to him for not giving up, when things did not work for no particular reason.

Thanks also to our postdoc Valery Milner for many discussions on physics, his help in daily lab work and for not eating the last chocolate truffle.

Daniel Steck has an amazing knowledge of physics that he is always willing to share. I am confident that he will eventually find out why diode lasers emit linearly polarized light. Thanks also for his never ending optimism on this project and the short introduction in "How to enter a highway."

Windell Oskay certainly needs less sleep than any other person I know. Thanks to him for spending some his time on answering questions about nearly everthing from optics through English grammar to movies and chocolate.

I also like to thank the people working on *the other experiment*. Martin Fischer translated weird English words that one never learns in school into

German and answered many questions on physics as well as computers. Todd Meyrath has a huge memory and uses part of it on such important things as Star Wars quotations. Todd, thanks for not forcing me to see "Hands on a hard body." Braulio Gutiérrez added another language to our lab as well as some nice discussions about senior lab and undergraduate education in the US among other topics.

For their help in proofreading and final editing of this work I like to thank Alexander Mück, Dan Steck, Mark Raizen and especially Windell Oskay.

Several other people have worked on making this year in Austin happen. Thanks to Prof. Dr. Scheer for creating the exchange program at the Universität Würzburg and Prof. Dr. Langhoff, Prof. Dr. Böhm and Prof. Dr. Yorke for their help and support during the organization period. I would like to acknowledge the financial support from the Deutschen Akademischen Austausch-Dienst.

Austin, August 4, 1999

MULTI-PASS AMPLIFICATION WITH A BROAD-AREA DIODE LASER

Nicole Helbig, M.A.
The University of Texas at Austin, 1999

Supervisor: Mark Raizen

This work describes the experimental investigation of amplifying a low-power single-mode diode laser with a high-power, broad-area diode laser. The goal of this method is to build a high-power single-mode laser system for further use in the cesium experiments in our lab. It is experimentally demonstrated that the method works, but the final goal of 0.5 W in a single mode has not been achieved thus far.

Table of Contents

Acknowledgments **v**

Abstract **vii**

List of Tables **xi**

List of Figures **xii**

Chapter 1. Introduction **1**

Chapter 2. Introduction to the Theory of Diode Lasers **3**
2.1 Basic Laser Physics 3
2.1.1 Gain Mechanism and Population Inversion 3
2.1.2 Resonator and Threshold 7
2.2 Diode Lasers 11
2.2.1 Principles 12
2.2.2 The GaAlAs Diode Laser 19

Chapter 3. Theoretical Description of Optical Systems **22**
3.1 Ray Tracing 22
3.2 Gaussian Beams 25
3.2.1 TEM_{00} Mode 25
3.2.2 Matrix Calculation for Gaussian Beams 27

Chapter 4. Theory of Multi-Pass Amplification **29**
4.1 Motivation 29
4.2 Theoretical Description 30

Chapter 5. The Experiment **36**
5.1 Setup 36
5.2 Alignment 41
5.3 Separating the Amplified Beam and Increasing its Intensity 44
5.4 Setup Components 47
5.4.1 Half-Wave Plate 47
5.4.2 Anamorphic Prism Pair 48
5.4.3 Optical Isolator 49

Chapter 6. Measurement Methods **51**
6.1 Knife-Edge Method 51
6.2 Spectrometer 53
6.3 Confocal Fabry-Perot Cavity 56

Chapter 7. The Diode Lasers **59**
7.1 Master Laser 59
7.2 Slave Laser 65

Chapter 8. Results **72**
8.1 Alignment and Beam Parameters 72
8.2 Input Angle 76
8.3 Driving Currents and Slave Temperature 81
8.4 Polarization 88
8.5 Dynamical Behavior 88

Chapter 9. Conclusions **90**

Appendices **93**

Appendix A. Mathematica Programs **94**
A.1 Ray Tracing 94
A.2 Gaussian Beams 95

Appendix B. Conversion of Resistance into Temperature **97**

Bibliography **99**

Vita **101**

List of Tables

B.1 Conversion of resistance into temperature for the used NTC-resistor 98

List of Figures

2.1 Basic interactions of light with matter 5
2.2 The working principle of a resonator 8
2.3 Band structure in different regions of the diode 13
2.4 Energy dependence of the level density N(E) 16
2.5 A simple laser diode 17
2.6 The layer structure of a heterojunction laser diode 20
2.7 The heterostructure 21

3.1 Ray tracing 23

4.1 Fabry-Perot model for multi-pass amplification 31
4.2 Ideal double-pass amplification 34

5.1 Experimental setup 37
5.2 Anamorphic prism pair 49

6.1 Knife-edge method 52
6.2 Example for the fit to a Gaussian beam 53
6.3 Schematic of our spectrometer 54
6.4 Diffraction grating 55
6.5 Schematic of a confocal Fabry-Perot cavity 56

7.1 Design of the master laser 61
7.2 Master laser spectrum 62
7.3 Measurement of active layer's width 67
7.4 Slave laser spectrum 68
7.5 Spectrum of slave and master laser 69
7.6 Center wavelength of slave laser 70
7.7 The effect of feedback 71

8.1 Vertical beam radius after spherical lens 73
8.2 Intensity in the amplified beam versus position of the spherical lens 74
8.3 Horizontal beam width after spherical lens 75
8.4 Amplification with large lens displacement 76
8.5 Spectra of the lasers 83
8.6 Spectra at 35 °C and 1.5 A driving current 84
8.7 Spectra at 45 °C and 2.0 A driving current 85
8.8 Spectra at 25 °C and 1.0 A driving current 86

Chapter 1

Introduction

Broad-area diode lasers are a reliable source for high power CW laser light. Unfortunately, the quality of the light does not meet the requirements of many experiments. The free-running output usually consists of several spatial as well as different temporal modes. Injecting a small amount of single spatial and longitudinal mode light into a broad-area diode has been shown to produce a high power output in a single mode by several groups [1–7]. Nevertheless, multi-pass amplification has not become a standard tool in physics and the knowledge about its ease of use is limited in spite of several publications. This work describes the results of our investigations of amplifying single-mode light with one specific broad stripe diode laser.

This project began with the ultimate goal of engineering a working laser system based on double-pass amplification that would be suitable for experiments with cold cesium atoms in our lab. The main motivation has been that diode lasers, compared for example with the argon-pumped Ti:Sapphire laser presently used, are easier to align and much cheaper to maintain. Not only is single mode light (spatial and longitudinal) required in the cesium experiments but also a power output of approximately 500 mW or higher is needed.

Here the physical limitations of diode lasers restrict their usefulness. Although high power laser diodes (well above 500 mW) are commercially available at the appropriate cesium transition wavelength (852 nm), single-spatial mode laser diodes typically have output powers below 100 mW.

The idea of double-pass amplification is to combine the best aspects of two diode lasers, one with single mode characteristics and one with high power output to accomplish all the needs of our experiment. In principle, a broad-area diode is simply used to amplify light in one mode injected by the second laser.

In 1988 Goldberg and Chun [3] showed that it is possible to gain 400 mW of single mode power out of a 1 W broad area diode. Therefore we expected that our ultimate goal of 500 mW was attainable with our 2 W laser diode. Thus far, we have not succeeded. Nevertheless, we have seen a lot of interesting physics in our experiments.

This work will start by introducing the basic physics underlying lasers and in particular diode lasers in Chapter 2 in order to form a solid basis for further discussion. The theoretical principles of beam propagation used throughout our work are discussed in Chapter 3. Chapter 4, about multi-pass amplification itself, finishes the theoretical considerations before we introduce the experiment in Chapters 5, 6 and 7. The results of our work and related analyses are presented in Chapters 8 and 9, where we conclude this work.

Chapter 2

Introduction to the Theory of Diode Lasers

This chapter explains some of the physical principles used in our experiment. First we give an overview of the general theory of the laser, and then we go on to explain the details of diode lasers.

2.1 Basic Laser Physics

Laser science is a broad topic that cannot be fully covered in this thesis. For a more general and complete discussion the reader is referred to [8–11].

We will briefly introduce the different components of a working laser system in this chapter. First, there is a gain medium, discussed in Section 2.1.1. We then consider the implications of the laser resonator in Section 2.1.2. Finally, there is the pumping mechanism of the laser. Because of the variety of possible pumping mechanisms, we shall restrict ourselves to the case of diode lasers, which we discuss in Section 2.2.

2.1.1 Gain Mechanism and Population Inversion

The basic physics of a laser can be explained most easily by making one crucial simplification, namely, that the gain medium (the heart of the laser) consists

only of two-level systems whose states are separated by an energy E_0. Naturally, this is not an exact description for any gain media especially because two-level systems cannot have population inversion in the steady state. Nevertheless, one can introduce all the basic physics in this model. We will restrict ourselves to two-level systems throughout this section and return to the complications of a realistic system when we discuss diode lasers in Section 2.2.

There are three different possible interactions between two-level systems and a radiation field consisting of photons. First of all, a photon can be absorbed if the lower level is occupied and the photon energy given by $E_\gamma = h\nu$ matches the energy difference between the two states: $E_\gamma = E_0$ (see Fig. 2.1a). This absorption is proportional to the intensity of light going through the considered medium because each photon has the same probability to be absorbed, σ, per unit length, per density N_1 of occupied lower levels. The probability σ is a property of the laser transition and can be calculated *ab initio* at least approximately in atomic or solid state physics. For low intensities, N_1 can be treated as a constant. For high intensity light, N_1 is reduced due to absorption that populates the upper level and becomes a function of position. This effect is often referred to as saturation. Therefore one should expect the following variation in the intensity I of a light beam when it goes through the medium in the x-direction:

$$dI(x) = -\sigma N_1(x) I(x) dx. \tag{2.1}$$

In the low intensity limit where N_1 is a constant, it is easy to calculate that the intensity of the beam after traveling a distance d will be

$$I(x_0 + d) = I_0 e^{-\sigma N_1 d}, \tag{2.2}$$

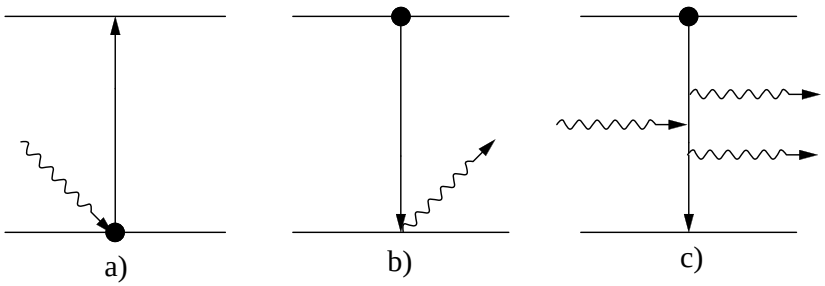

Figure 2.1: Basic interactions of light with matter: A two level system can (a) absorb light while in the lower state and (b) spontaneously emit light while in the upper state. A photon can stimulate emission (c) while the upper state is occupied.

where $I_0 = I(x_0)$. This exponential damping is usually observed when light passes through any medium. The damping coefficient σ is high in opaque and low in transparent materials. If the assumption of low intensities breaks down, saturation effects will decrease the effective absorption and change the exponential damping law.

When the system is already in the upper state, the process of spontaneous emission comes into play (see Fig. 2.1b). In this process the system can decay by emission of a photon into the lower state with a rate unaffected by the intensity of a photon field. This type of interaction can be very weak in comparison with stimulated emission, which will be discussed later.

Now we can specify more precisely what we mean by low intensity in the discussion of absorption: the rate of absorption, which is proportional to the intensity, has to be very small compared with the spontaneous emission rate. Only in that case will the change of N_1 due to this absorption be negligible.

The third interaction process between matter and radiation is stimu-

lated emission (see Fig. 2.1c). Whenever light of the right frequency ($\nu = E_0/h$) passes through material that consists of systems partly in the upper level, it induces transitions to the lower level by coherent emission of photons. Coherent means that the electromagnetic wave associated with the photon has the same wave vector and phase as the incoming wave (i.e., there is complete constructive interference). It turns out that the change of the light intensity in the low-intensity limit is $I(x_0 + d) = I_0 e^{+\sigma N_2 d}$, where N_2 is the density of occupied upper levels. Here, low intensity means that there is a process (pumping) that reoccupies the upper level with a rate higher than that of stimulated emission.

The ratio of stimulated to spontaneous emission in an external field is approximately equal to the number density of photons in the field, which can be made very high. Therefore, effects of spontaneous emission can be usually ignored in calculating the variation of intensity in a medium.

Naturally, both levels are partially occupied in any medium and the combined absorption and stimulated emission lead to the following intensity change for a light ray:

$$I = I_0 e^{-\sigma(N_1 - N_2)x}. \tag{2.3}$$

In typical matter it is more probable that the lower level is occupied, as one might expect from a Maxwell-Boltzmann distribution. Therefore, light is usually absorbed in matter as stated before, but if N_2 is larger than N_1, one gets Light Amplification by the Stimulated Emission of Radiation (i.e., a LASER). A medium with this property is often referred to as an active or gain medium.

For a physicist or laser engineer the essential task is now to achieve this population inversion by finding a pumping mechanism to populate the upper level by more than 50%. As discussed before this population inversion cannot be achieved in a two-level system. We will return to this topic in Section 2.2. First, however, we want to discuss the laser's resonator because without any resonator system the active medium would emit more or less isotropically (depending only on the geometry of the gain medium) with low intensity and little coherence.

2.1.2 Resonator and Threshold

In order to get high intensities in a directed beam the distance the light travels in the gain medium should be as large as possible in one distinct direction. Therefore it is natural to use mirrors to reflect the already amplified beam back into the medium for further amplification to take advantage of the (essentially) exponential amplification law (2.3).

Let us first assume the simplest case, namely plane mirrors on both sides of the active medium. A beam started by spontaneous emission perpendicular to the mirrors' surfaces is amplified and reflected back to be amplified again and so on. Nearly all light generated by spontaneous emission is not perpendicular to the mirrors and leaves the cavity quickly. It is not amplified much because of its short path through the active medium (see Fig. 2.2).

Besides the variation of intensity according to equation (2.3) there are also losses because the reflectivity of the mirrors' surfaces is not perfect. Further, the finite dimension of both the mirrors and the gain medium lead to

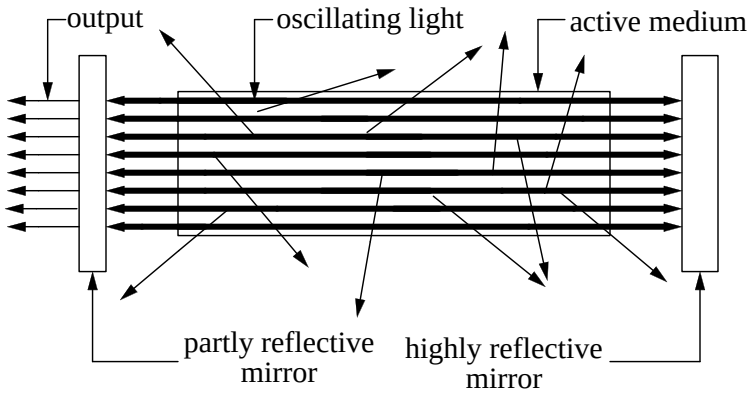

Figure 2.2: The working principle of a resonator: Light traveling perpendicular to the mirrors is amplified while oscillating between the two mirrors. The left mirror is used to couple a certain amount of light out to produce the laser beam. Light in other directions leaves the cavity quickly without large amplification.

losses from various diffraction effects. Finally, one can include losses due to absorption followed by spontaneous emission. If we assume that during each round trip through the cavity a certain fraction of the light L is lost through these mechanisms, the ratio of the intensity to the initial intensity after one round trip is

$$\frac{I}{I_0} = Le^{\sigma(N_2-N_1)d} \tag{2.4}$$

where d is the length of a single round trip through the active medium. It is easy to see that lasing can only occur if the ratio in Equation (2.4) is larger than unity, because only that case will build up the intensity.

Of course the growth in intensity per round trip according to Equation (2.4) cannot go on forever. The low intensity limit eventually becomes invalid because the pumping process is no longer efficient enough. The population density N_2 decreases homogeneously throughout the medium (such that

Equation (2.4) still holds but with a reduced $N_2 - N_1$) to a point where the gain equals the loss per cycle. At this point a stationary intensity I_{S} is established in the cavity. From these considerations the output power P_{laser} of a laser is given by

$$P_{\mathrm{laser}} = T \int_{\text{mirror surface}} I_{\mathrm{S}} dA \tag{2.5}$$

where T is the transmittance of the output mirror and the integral is over the stationary intensity of the beam profile.

So far we have not discussed the consequences of coherence in the laser's resonator. Because of the coherence in stimulated emission we have to take into account interference effects of the waves in between the two mirrors. A first major consequence of this interference is that in a given resonator amplification can only be achieved for frequencies that fulfill the condition for a standing wave,

$$\nu_l = \frac{c_{\mathrm{m}} l}{2L}. \tag{2.6}$$

Here, c_{m} is the speed of light in the laser medium, L is the distance between the two mirrors and n can be any positive integer. This expression is only exact if the active medium fills the whole space between the mirrors ($L = \frac{d}{2}$); otherwise, one has to take the different refractive indices (leading to different c_{m}'s) into account. These frequencies are frequently referred to as longitudinal modes of a laser and lead to complete constructive interference. At all other frequencies destructive interference between different parts of the electromagnetic field propagating between the mirrors inhibits laser oscillation.

If the transitions between the two levels in our simplified system would be possible only at a single, well defined energy (as assumed thus far), it would lead to the stringent requirement that the resonator must exactly match the corresponding frequency. Fortunately, every physical transition used in lasers has a certain finite linewidth about its center frequency. That is to say that σ is a function of the frequency ν, with typically a Lorentzian profile with the center at the energy separation of the transition as familiar from atomic physics.

The quantity n in Equation (2.6) is usually very large ($n > 500$ even in small diode lasers) and therefore $n + 1$ does not differ very much from n. Thus, the longitudinal modes are close to each other and many frequencies ν_{n} can actually be amplified. This effect will be discussed in greater detail in Section 2.2.

The resonator does not only restrict lasing to longitudinal modes but also forms certain transverse modes (i.e., amplitude or intensity distributions perpendicular to the direction of beam propagation), often referred to as TEM modes (Transverse ElectroMagnetic modes). To allow constructive interference, the amplitude distribution A on one of the mirror surfaces must equal the distribution after one round trip in steady state. This condition leads to an integral equation from Fourier optics,

$$A(\tilde{x}, \tilde{y}) = c\frac{i}{2\lambda} \int_x \int_y A(x, y) \frac{1}{r} e^{-ikr}\, dx\, dy, \tag{2.7}$$

where λ is the wavelength of the longitudinal mode, k is its wave vector, and r is the round-trip distance between the two points on the mirror specified by $(\tilde{x}, \tilde{y})$ and (x, y).

Equation (2.7) leads to different solutions for different cavity types (e.g., plane or confocal Fabry-Perot cavities) and to different possible modes for each cavity. As an example of how mathematically complicated these modes may become, we present here the solution for a stable cavity as derived for example in [8]

$$\begin{aligned} E_{ij}(x,y,z) \propto & H_i\Big(\frac{\sqrt{2}x}{w(z)}\Big) H_j\Big(\frac{\sqrt{2}y}{w(z)}\Big) \\ & \exp i[kz - (i+j+1)\tan^{-1} z/z_0] \\ & \exp ik(x^2+y^2)/2R(z)\ \exp -(x^2+y^2)w^2(z). \end{aligned} \tag{2.8}$$

Here, $w(z)$ is the beam radius, $z_0 = \pi n w_0^2/\lambda^2$, where w_0 is the beam radius at $z = 0$. $R(z)$ is the curvature of the beam (all these parameters are discussed in more detail in Section 3.2). H_i and H_j stand for the Hermite polynomials of order i and j. The indices i and j are used to label the different TEM modes (e.g., E_{00} is denoted by TEM_{00}). The resulting intensity profile is of a Gaussian form and therefore leads to Gaussian beams (see Section 3.2). We will now move on and discuss the physics of diode lasers in more detail.

2.2 Diode Lasers

A diode laser relies on the properties of a p-n junction that may be familiar from normal p-n junction diodes in electronics. We will first look at the basic physical principles that allow the usage of such a semiconductor device as a laser in Section 2.2.1, and then we will look at the special examples of the lasers used in our experiment in Section 2.2.2.

2.2.1 Principles

First of all, it is essential to understand how our two-level system introduced in 2.1.1 might be realized in diode lasers. In semiconductor materials the valence and conduction bands are well separated by an energy gap of roughly 1 eV. The two levels that can be coupled by radiation are therefore both an electron in the valence band and a hole in the conduction band (the lower level in the two level model) or an electron in the conduction band and a hole in the valence band (the upper level in the two level model). The holes are crucially important because an electron can make a transition only into an unoccupied state in the conduction or valence band because of the Pauli principle.

In an n-type doped semiconductor there are many electrons in the conduction band and no holes in the valence band (see Fig. 2.3a), and in the p-type material the opposite is true (see Fig. 2.3b). In the region near a p-n junction the nearby electrons and holes diffuse into each other's domain, recombine (see Fig. 2.3c), and a potential barrier builds up to prevent unlimited diffusion. This process is known from basic solid state physics and is essentially enough to lay the foundations for a potential lasing capability of this system. For a more complete discussion of semiconductors and p-n junctions see, for example, the book by Ashcroft and Mermin [12].

Outside of the recombination region, no two-level systems with energy separations close to the band gap are formed (there may be holes in the valence band or electrons in the conduction band, but again, both cases are necessary to form the two-level system). Inside this region, predominantly the lower level is occupied.

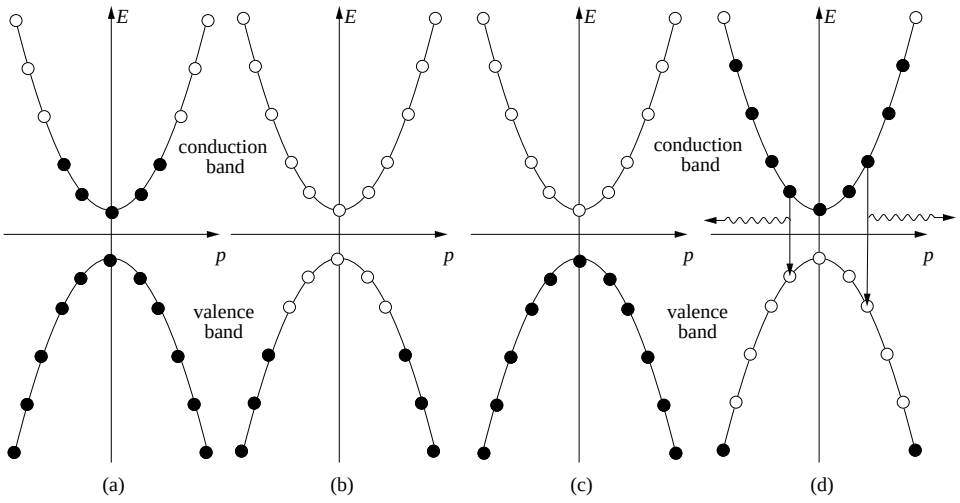

Figure 2.3: Band structure in different regions of the diode drawn in a simple harmonic approximation (black and white dots show electrons and holes respectively). Shown are examples of (a) an n-type doped material and (b) a p-type doped material. (c) In the absence of externally applied fields light-emitting transitions can not occur at the p-n junction. (d) In a forward-biased p-n junction, electron-hole pairs can radiatively recombine.

Of course, this system is far from our previously assumed two-level picture because a solid-state energy band, as the name suggests, consists of quasicontinuously distributed states in a certain energy interval. This results in a fairly broad energy range in which optical transitions can occur between states within this band structure. This situation is in contrast to a gas laser where only one transition (with a fixed center frequency) can lase, a semiconductor has two-level systems with continuously varying energy separations. The minimum energy in this range equals the band gap of the given semiconductor. Therefore, the density of two-level systems is a function of center frequency ν of photons emitted or absorbed by the corresponding transition, which has its own natural linewidth. We shall note here that for example

an electron in the conduction band can contribute to the density of two-level systems $N(\nu)$ in a whole frequency region because it can recombine with different holes at different energies. The level density $N(\nu)$ as a function of ν is in general complicated as is the band structure of real materials.

Let us consider the case where essentially only the lower levels are occupied as occurs for thermal equilibrium within the p-n junction. In this regime light with a photon energy slightly larger than the gap energy can be absorbed efficiently because $N(\nu)$ is large and approximately equals $N_1(\nu)$. In GaAs (discussed in Section 2.2.2) the absorption coefficient $\sigma(N_2 - N_1)$ is as large as 1170 cm^{-1} in the near infrared; hence, light in that frequency range can penetrate this material only approximately 10 μm.

The density of occupied upper levels can be dramatically changed by forward-biasing the diode. This corresponds to the pumping necessary for a laser as mentioned in Section 2.1.1. An external electric field can overcome the potential barrier in the p-n junction and drive both conduction-band electrons and valence-band holes from the n-type and p-type regions, respectively, into the p-n junction. The density of occupied upper levels then rises because the electrons are driven into this region more quickly than they recombine with the holes. Ideally, one can achieve a situation as shown in Fig. 2.3d where all states in the conduction band up to a certain energy are occupied by electrons and the corresponding states in the valence band contain holes. In other words, if the rate of electrons and holes entering the recombination region is large enough the pumping will be so effective that $N_1(\nu)$ is essentially zero and $N(\nu) \approx N_2(\nu)$. When the population inversion condition is satisfied, light

in the appropriate frequency range will cause stimulated emission. The light intensity will increase exponentially with the same coefficient of 1170 cm^{-1}. These conditions are optimal for a laser.

Naturally, recombination processes due to these stimulated emissions or other optical or vibrational processes will drastically reduce the population inversion, but nevertheless a large stationary density $N_2(\nu)$ in a certain frequency region can remain. Hence, the gain can still be quite large in semiconductor lasers where gain factors above 10 per round trip are common.

We can now estimate the functional dependence of $N_2(\nu)$ and, assuming that $\sigma(\nu)$ is approximately constant, the gain of a laser using such a p-n junction as active medium. Furthermore, let us assume complete inversion in a certain region ΔE above the band gap. Directly at the gap energy only a few electron-hole pairs can undergo stimulated emission because electrons above the lower band edge cannot find holes with the right energy difference for recombination. For the maximum energy where stimulated transitions are possible, the situation is similar (see Fig. 2.4a). However, at a certain energy in between these extreme cases, nearly every electron in the valence band can recombine with a corresponding hole at the correct energy separation (see Fig. 2.4b), and the gain is optimized. This qualitative picture with a peak gain at a frequency slightly higher than the band gap (see Fig. 2.4c) is close to both the results of detailed calculations as given, for example, in [13] and to our experimental results (see Section 7.2).

Of course, there are always electrons in the valence band far below the band edge (see Fig. 2.3d), and so the semiconductor remains opaque above a

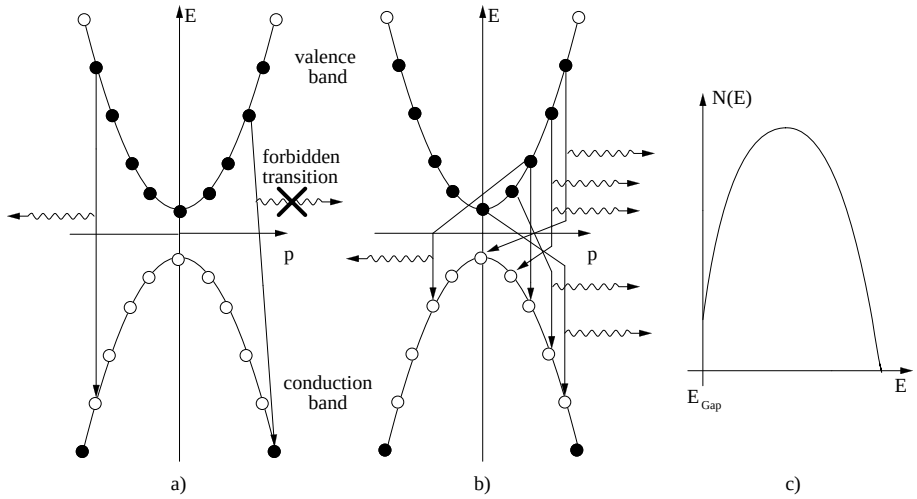

Figure 2.4: Energy dependence of the level density $N(E)$: (a) transitions at the highest energy where pumping is still effective. $N_2(E_{\max})$ is low because most of the electrons cannot make transitions to the valence band. (b) At a certain energy nearly every electron can find a hole to recombine with and $N(E_{\text{optimal}})$ is large. (c) shows a qualitative picture of $N_2(\nu)$

certain frequency. However, the window of optical transitions with energies close to the band gap energy which cannot couple to these electrons is large enough to make the construction of a laser possible.

The electron and hole flux through the junction results in a current I through the diode, often referred to as the driving current. The power P_{pump} contained in the produced photons and phonons (vibrational excitations of the crystal due to non-optical processes) is pumped into the system through the external voltage V and equals the voltage drop across the junction V_{junction} times this current:

$$P_{\text{pump}} = IV_{\text{junction}}. \tag{2.9}$$

A remaining step in the construction of a diode laser system is the

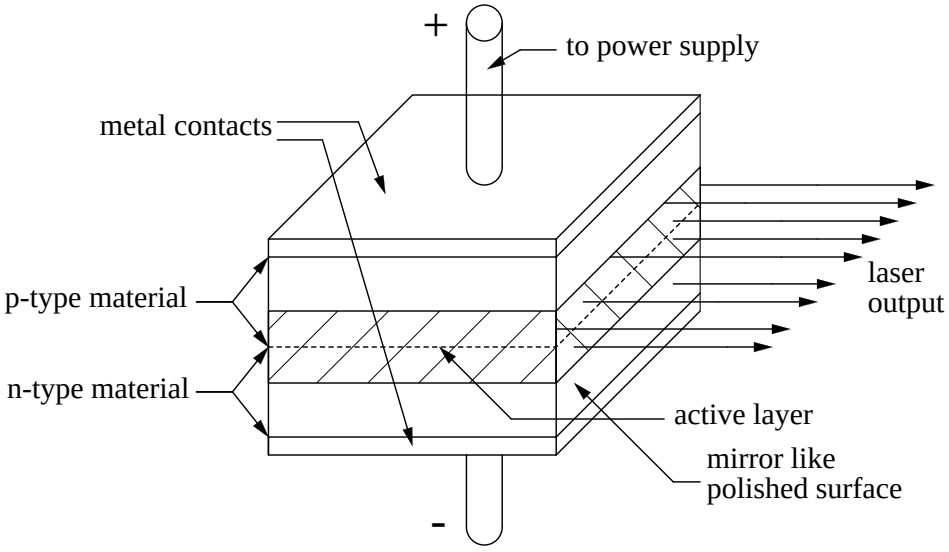

Figure 2.5: A simple laser diode consisting only of two semiconductor layers and metal surfaces to apply the external voltage. The active region and the region of light output are not well defined.

resonator. One way to construct a resonator is to polish two of the surfaces of the diode (Fig. 2.5). These surfaces tend to be reflective because of the change in the index of refraction. The gain in a diode laser is usually high enough that efficient reflection is not always necessary. If needed, one can coat the surfaces to improve or suppress reflection.

Compared with gas lasers, the cavity in a diode laser is very short. The dimensions of the diode itself are usually in the submillimeter range. Therefore two adjacent longitudinal modes are typically much further separated than in other laser systems (see Equation (2.6)).

Taking into account the properties of the system, one can, in principle, calculate the stationary intensity I_S in the laser cavity as well as the output

intensity. These intensities depend on $\sigma(\nu)$ and the stationary value of $N_2(\nu) - N_1(\nu)$, as in Equation (2.4) with $I/I_0 = 1$. Therefore, I_S is naturally also a function of frequency. $N_2(\nu) - N_1(\nu)$ will be roughly proportional to the driving current because it repopulates the upper level while stimulated transitions try to lower $N_2(\nu)$. A certain threshold current is thus needed to start the lasing of the system. Besides the lower limit on current established by the threshold, damage mechanisms related to high current and power place an upper limit on the current applied to the diode.

The measured spectrum of one of the diode lasers in our experiment is shown in Fig. 7.4 as an example of a real diode laser. The functional dependence of the stationary intensity $I_S(\nu)$ on frequency is reflected in the different intensities of the various amplified longitudinal modes. Lasing occurs within approximately a 2 nm band. Outside of this band the frequencies are not amplified sufficiently to start laser oscillation and absorption processes are dominant at frequencies even further away.

The band gap energy depends on both temperature and the driving current, and so the center of the amplification region is also a function of these parameters, as discussed in Section 7.2. Further, the separation of the longitudinal modes can change because the speed of light in the medium and the cavity length depend upon temperature and driving current (see Equation (2.6)).

There are, of course, challenges in actually realizing a diode laser. First of all, the non-optical transitions reduce the population inversion and therefore the gain. A second problem is that the active region (the region of population

inversion) is not well defined, because the electrons and holes are not confined to a certain region but undergo diffusive motion. The carriers may then leave the lasing region before recombination and therefore decrease N_2 in the lasing region. Methods for overcoming these problems are discussed in Section 2.2.2.

2.2.2 The GaAlAs Diode Laser

Some of the problems mentioned in Section 2.2.1 can be solved by the appropriate choice of materials. Here GaAlAs is a suitable semiconductor for the purpose of designing a laser diode for use in the near infrared. The band gap energy corresponds to a wavelength in this region and is therefore near the cesium transition ($\lambda = 852$ nm) that we are interested in. Furthermore, the efficiency in optically converting electron-hole pairs in the active layer is nearly unity. Therefore the overall efficiency $\eta = \frac{P_{\text{laser}}}{P_{\text{pump}}}$ is also higher than for other systems. This implies that the heating of the diode due to the driving current is relatively small. This efficiency is a major advantage since heat production reduces the lifetime of semiconductor lasers.

So far, we have only considered the simplest possible p-n junction, a so-called homojunction where the same semiconductor material is used for both the n- and p-type regions. One can also build slightly more complicated diodes, heterojunctions, which consist of different semiconductor materials. In the GaAlAs system these different materials are $\text{Ga}_i\text{Al}_{1-i}\text{As}$ layers with different i values. One example of a common layer structure of such a heterojunction is shown in Fig. 2.6.

There are three major advantages in a system where a parameter like i

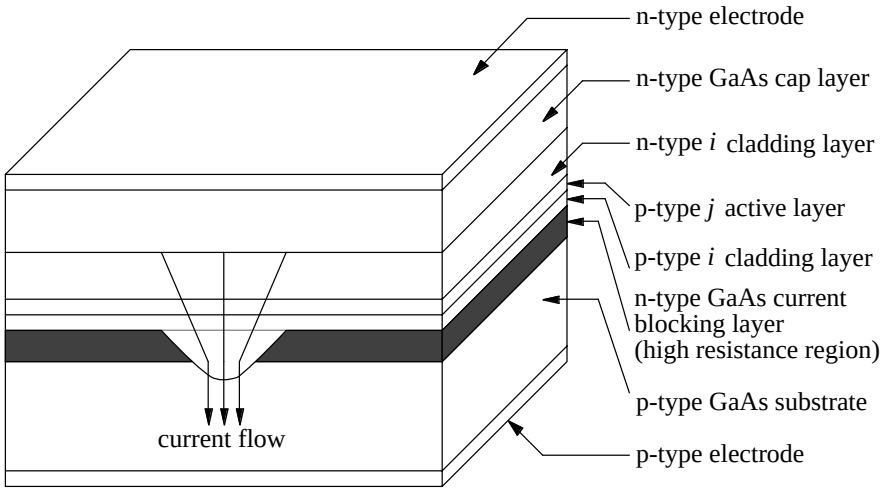

Figure 2.6: The layer structure of a heterojunction laser diode: i stands for $Ga_iAl_{1-i}As$, j for $Ga_jAl_{1-j}As$. Both materials have different band gap energies and refraction indices with interesting consequences: only the active layer produces light output (see text below); the blocking layer further confines the region of population inversion in the direction parallel to the active layer.

can be varied. First, the band gap energy is a function of i, and therefore the wavelength of the laser can be selected within a certain range. Furthermore, if the active layer is different from the surrounding, "cladding" layers, the index of refraction is generally different, and with a suitable choice of parameters the active layer can be used as a wave guide to confine the laser light within the active layer itself. Finally, i-dependent band gaps can be used to obtain a well-defined active layer because they provide an effective barrier to diffusion of carriers out of the active layer (see Fig. 2.7). All these properties make GaAlAs useful in semiconductor laser technology.

The different bandgap energies confine the active layer in the direction perpendicular to the layer. A confinement in the parallel direction can be

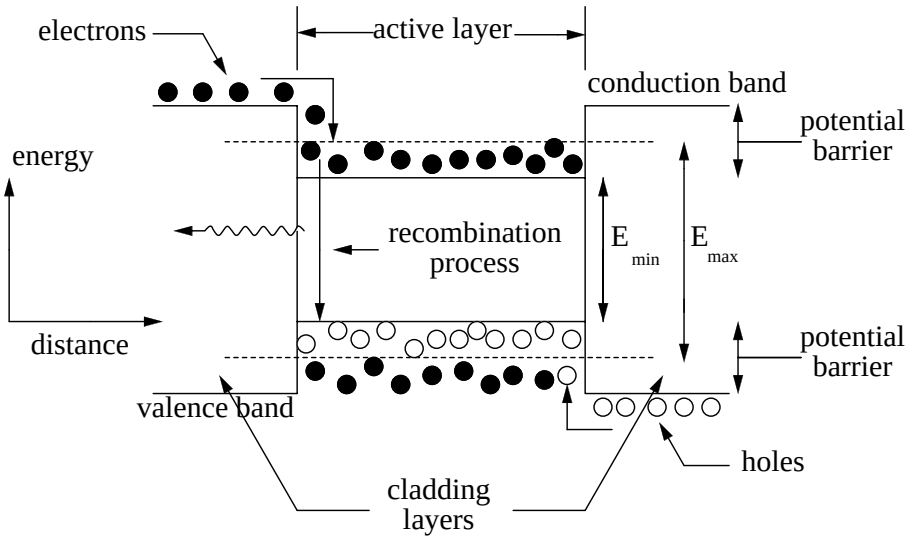

Figure 2.7: The heterostructure: electrons and holes are driven by the external electric field but the reduced band gap in the active layer provides a potential barrier that confines them. Transitions can only occur within this low-potential region. The materials one can use for the different layers in order to produce such a structure are the same as in Fig. 2.6.

achieved by including an additional high-resistance region that restricts the current flow in this direction. This confinement results in population inversion only occurring within a specific stripe (see Fig. 2.6). The effects of different stripe widths on the output beam characteristics will be discussed in Section 4.1.

Chapter 3

Theoretical Description of Optical Systems

Finding the optimal alignment of a system containing a large number of optical elements on a table can easily become complicated and time consuming. Fortunately, there is a theoretical approach for calculating the path (described in Section 3.1) and the characteristics (described in Section 3.2) of a propagating beam. For Gaussian beams, the calculations are particularly easy and we will restrict ourselves to the discussion of Gaussian beams here because the beams in our experiment can be well approximated as Gaussian.

3.1 Ray Tracing

Let us first consider the propagation of light in the limit given by geometrical optics. That means that we describe a beam as a ray, and we ignore diffractive effects due to the finite beam width. Therefore, the beam can be completely described by its distance r from the optical axis and its direction. In more mathematical terms, the direction is specified by the slope r' of the ray when plotted against its distance along the optical axis, which is parameterized by a coordinate z. We are interested in calculating the two functions $r(z)$ and $r'(z)$ along the whole optical axis in order to obtain complete information about

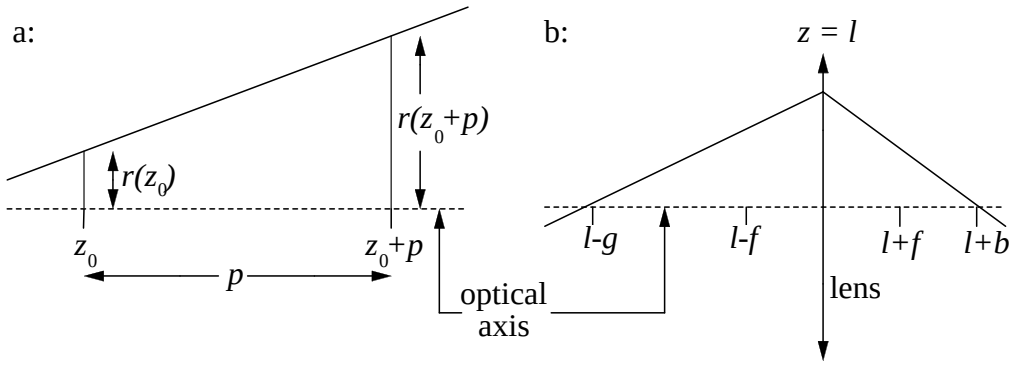

Figure 3.1: Ray tracing: (a) Propagation over a free path of length d. The light ray just forms a straight line with $r' = \text{constant} = (r(z_0 + d) - r(z_0))/d$. (b) Propagation through a lens of focal length f. The slope $r'(z)$ jumps at $z = l$.

the location and direction of the beam everywhere in the setup. To simplify the picture further, we will assume nearly paraxial light rays (i.e., the beam is propagating close to the optical axis and at only small angles).

From Fig. 3.1a it can be seen that free propagation between different optical elements can be described easily. The beam parameters at two different points along the optical axis separated by a distance d are simply related by

$$\begin{aligned} r(z+d) &= r(z) + d \cdot r'(z) \\ r'(z+d) &= r'(z). \end{aligned} \tag{3.1}$$

In matrix notation, we have

$$\begin{pmatrix} r(z+d) \\ r'(z+d) \end{pmatrix} = \begin{pmatrix} 1 & d \\ 0 & 1 \end{pmatrix} \begin{pmatrix} r(z) \\ r'(z) \end{pmatrix}. \tag{3.2}$$

For a thin lens with focal length f, the picture looks a little different (see Fig. 3.1b). The lens is assumed to have zero thickness and its physical effect is described by a sudden change in the propagation direction at the

lens. We therefore introduce $r_{\mathrm{in}}(l)$, $r'_{\mathrm{in}}(l)$ and $r_{\mathrm{out}}(l)$, $r'_{\mathrm{out}}(l)$ to describe the discontinuous change, where l is the coordinate of the lens. From Fig. 3.1b one can easily extract the beam parameters

$$\begin{aligned} r_{\mathrm{in}}(l) &= r_{\mathrm{out}}(l) \\ r'_{\mathrm{in}}(l) &= \frac{r_{\mathrm{in}}(l)}{g} \\ r'_{\mathrm{out}}(l) &= -\frac{r_{\mathrm{out}}(l)}{b}. \end{aligned} \tag{3.3}$$

This results in

$$\begin{aligned} \frac{1}{f} &= \frac{r'_{\mathrm{in}}(l)}{r_{\mathrm{in}}(l)} - \frac{r'_{\mathrm{out}}(l)}{r_{\mathrm{in}}(l)} \\ \Rightarrow r'_{\mathrm{out}}(l) &= -\frac{1}{f} r_{\mathrm{in}}(l) + r'_{\mathrm{in}}(l), \end{aligned} \tag{3.4}$$

where we have used the fact that $1/f = 1/g + 1/b$ with g and b the distance between the lens and the object and the lens and the image respectively. One can write this again in matrix notation as

$$\begin{pmatrix} r_{\mathrm{out}}(l) \\ r'_{\mathrm{out}}(l) \end{pmatrix} = \begin{pmatrix} 1 & 0 \\ -\frac{1}{f} & 1 \end{pmatrix} \begin{pmatrix} r_{\mathrm{in}}(l) \\ r'_{\mathrm{in}}(l) \end{pmatrix}. \tag{3.5}$$

Another important optical component is a flat mirror, which can be ignored because it deflects the optical axis in the same way as the beam and therefore has no overall effect. Curved mirrors with radius R can be included as lenses with the corresponding focal length $R/2$.

Starting from some initial condition, the beam parameters at any point in the setup can be obtained simply by calculating the changes due to optical elements and free propagation up to that point. In our matrix notation we can write

$$\begin{pmatrix} r(z) \\ r'(z) \end{pmatrix} = \begin{pmatrix} A & B \\ C & D \end{pmatrix} \begin{pmatrix} r_{\mathrm{initial}} \\ r_{\mathrm{initial}} \end{pmatrix}. \tag{3.6}$$

where this general matrix is naturally given by the matrix product of all the matrices corresponding to propagation and optical elements in the order of the setup (written from right to left).

3.2 Gaussian Beams

So far, we have only discussed beams in terms of geometrical optics. This approach is only appropriate for a beam width large compared to the wavelength so that one can neglect diffraction effects and is used in the case that one is not interested in the beam width itself. Since we sometimes work with focused beams and the beam width is an important property for us, both conditions are violated and we must include these effects in our calculations. This complicates the discussion in general, but it turns out that the behaviour of Gaussian beams can be computed in a straightforward manner. Treating the beams in our experiment as Gaussian is a fairly good approximation; so, this method is quite useful, and we will introduce it in this section.

3.2.1 TEM_{00} Mode

The basic property of a Gaussian beam, as the name suggests, is that its transverse intensity profile is a cylindrically symmetric Gaussian. This profile can be found for example in a TEM_{00} mode of a laser (see Section 2.1.2). There are again two characteristics of the beam we want to know as it propagates along the optical axis. One is the beam width mentioned before (the full width of the profile where the electric field has dropped to $1/e$). The second is the divergence of the beam to be defined below.

By directly solving Maxwell's equations in a homogeneous material with index of refraction n (with an initial Gaussian intensity distribution and using a slowly varying amplitude approximation) one can get the functional dependence of the electric field propagating in z-direction on the spatial coordinates. A detailed calculation as given in [14] yields the result

$$\begin{aligned}\frac{E(r,\phi,z)}{E_0} &= \frac{w}{w(z)}\exp\Big(-\frac{r^2}{w^2(z)}\Big) && \text{(amplitude factor)}\\ &\times \exp\Big(-i\Big[kz-\tan^{-1}\Big(\frac{z}{z_0}\Big)\Big]\Big) && \text{(longitudinal factor)}\\ &\times \exp\Big(-i\frac{kr^2}{2R(z)}\Big), && \text{(radial phase)}\end{aligned} \tag{3.7}$$

where $w(z) = w_0\Big(1+\Big(\frac{z}{z_0}\Big)^2\Big)^{\frac{1}{2}}$ denotes the beam radius, $R(z) = z\Big(1+\Big(\frac{z_0}{z}\Big)^2\Big)$ is the curvature of the beam, $z_0 = \frac{\pi n w_0^2}{\lambda_0}$, λ_0 is the wavelength of the light, and w_0 is the beam radius at $z = 0$.

Since we are only interested in the beam width and divergence and not in phase factors let us focus on the amplitude factor. Clearly $w(z)$ is the beam radius as defined before. Furthermore, one can see that $w_0 = w(0)$ is the minimum beam radius and that $w(z_0) = \sqrt{2}w_0$. The factor $\frac{w_0}{w(z)}$ in front of the exponential makes sure that the power in our beam is conserved, which is quite satisfying since we have obtained this result without including any absorption effects.

At this point we have succeeded in assigning a variable to one of our two needed parameters. We are now left with the divergence of the beam. For $z \gg z_0$ one can neglect the first term in $w^2(z)$ such that the formula simplifies to

$$w(z) = \frac{w_0 z}{z_0} = \frac{\lambda_0 z}{\pi n w_0}. \tag{3.8}$$

Therefore, $w(z)$ is proportional to z for large z. The divergence δ can be characterized by the constant of proportionality

$$\delta = w'(z) = \frac{\lambda_0}{\pi n w_0}, \tag{3.9}$$

or the angle $\theta = \frac{2\lambda_0}{\pi n w_0}$ the beam propagates into.

3.2.2 Matrix Calculation for Gaussian Beams

Equation (3.7) shows how to calculate the beam width $w(z)$ and the divergence of a beam in free space, but what effect will optical components have on such a Gaussian beam? It turns out that there is a parameter $q(z)$ defined by

$$\frac{1}{q(z)} = \frac{1}{R(z)} - i\frac{\lambda_0}{\pi n w^2(z)} \tag{3.10}$$

that can be calculated throughout an optical setup according to the $ABCD$ law:

$$q(z) = \frac{Aq_{\text{initial}} + B}{Cq_{\text{initial}} + D} \qquad \text{or} \qquad \frac{1}{q(z)} = \frac{C + D \cdot (1/q_{\text{initial}})}{A + B \cdot (1/q_{\text{initial}})} \tag{3.11}$$

where A, B, C and D correspond to those in Equation (3.6) for the same setup. One justification for this equation is that detailed calculations as given in [14] for each optical component yield the same result as this equation. A formal proof for the validity of this law is given in [15].

Since the imaginary part of $1/q(z)$ is proportional to $1/w^2(z)$, this equation is useful in computing the beam width, given some initial value. The divergence of the beam can be calculated easily from the minimum beam width w_0 and Equation (3.9).

The matrices given in Section 3.1 together with Equations 3.6 and 3.11 were used in Mathematica® to calculate beam paths and beam widths with

the appropriate experimental setup as input. The code for these calculations is given in Appendix A.

Chapter 4

Theory of Multi-Pass Amplification

Having described some physical background about lasers in general and diode lasers in particular in Chapter 2, we are now ready to introduce the physics of multi-pass amplification itself. We will first discuss why this method is promising in diode laser technology and then introduce a theoretical model that describes it.

4.1 Motivation

In order to explain the potential of double-pass amplification, we need to discuss the limitations of diode lasers first.

Diodes with a broad active layer tend to oscillate in many different spatial modes. One can overcome this problem by confining the active, amplifying region to a narrow stripe as described in Section 2.2.2. This technique is effective and it is possible today to produce diodes with a single spatial mode. A diode can also be made to oscillate in a single longitudinal mode, that is, at a single frequency, by applying a feedback mechanism. Feedback can be provided, for example, by an external grating as described in Section 7.1. While a laser can be made to exhibit single-mode behavior, it is often at

the expense of output power.

Ideally, the output power of a laser diode would increase monotonically with increasing driving current, but there is a strict limitation for this current and therefore the output intensity. For high enough output power the light intensity oscillating in the semiconductor crystal may become so large that it damages the facet of the diode crystal that is used to couple the intensity out. Defects in the regular semiconductor structure begin to spread at these intensities and may cause an irreversible destruction of the resonator and the whole diode. The overall output power is in simple terms the integral of the output intensity over the area of the laser diode facet where light is emitted (see Equation (2.5)). It is thus reasonable that in diodes with broader front facets larger total output powers can be achieved.

In applications where both single-mode characteristics and high power are necessary, neither of the two extremes is sufficient. This is where multi-pass amplification comes into play as a useful tool. In principle, it should be possible to use a high-power diode to amplify single-mode light from a single-mode "master" laser.

4.2 Theoretical Description

We are finally in a position where we can discuss the physical principles underlying our experimental efforts. Multi-pass amplification is a complicated process involving the dynamics of a broad-band laser diode and its response to injected light.

The dynamics of free-running broad-area diodes are discussed, for ex-

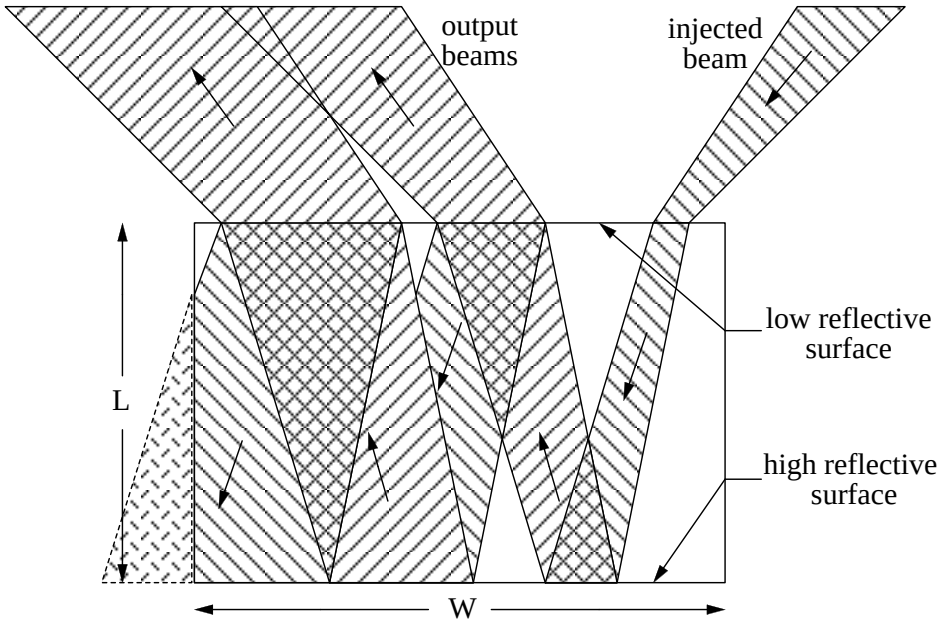

Figure 4.1: Fabry-Perot model for multi-pass amplification, light is refracted at the front facet of the diode according to Snell's law and then propagates freely in the medium. A certain fraction of the intensity is emitted as a Gaussian beam after each round trip. On the left edge of the active layer attenuation is assumed without reflection. The ratio $\frac{L}{W}$ is usually around 3 (not to scale for clarity).

ample in [16], and exhibit spatiotemporal chaos. The numerical calculations in [16] are very involved and do not include external light injection. We will therefore approach the problem of multi-pass amplification by describing the broad-area diode as a saturated amplifier following a much simpler description given in [2].

In this model, the broad-area diode's active layer can be simply described as a large, two-dimensional Fabry-Perot cavity. (For a detailed description of a Fabry-Perot cavity see Section 6.3.) Here, two-dimensional means

that the injected beam can be described as wave-guided and therefore confined in the dimension perpendicular to the active layer by the diode's heterostructure, as introduced in Section 2.2.2. Within these two dimensions it propagates freely in the semiconductor medium characterized only by the index of refraction. Because of the typically small waist of the injected beam, the light will diverge slightly, resulting in overall behavior as shown in Fig. 4.1.

Amplification due to stimulated emission is introduced by hand in the model by assuming a certain amplification of the incoming beam while propagating to the reflective rear facet of the diode and back. It will be naturally limited by the gain factor of the light oscillating in the free running modes. That is, corresponding to Equation (2.4) and ignoring all other losses, the amplification is the inverse of the front reflectivity of the active medium. Therefore, the lower the reflectivity of the front facet the better the initial conditions for a large amplification of injected light.

If the injected intensity is small compared with the stationary intensity in the free running modes it should not have a major impact on the population inversion and therefore the gain factor of the active medium. In this scheme it is then natural to assume that the gain, including all the losses (especially at the relatively transparent front facet), is simply unity for all of the following round trips. That means that the injected light simply behaves like the free running light according to Equation (2.4).

Once the injected beam reaches the left or right edge of the active layer it is assumed to be attenuated, since without population inversion the semiconductor heavily damps the intensity. No reflection occurs because the

difference in indices of refraction between the pumped and unpumped regions of the same layer is small.

Taking into account the preceding considerations, this model predicts that the outgoing intensity due to external injection can be described using overlapping and interfering Gaussian beams. The interference between the beams reflects the coherence in the amplification process in the active layer. The beams themselves can be described as discussed in Section 3.2 with an additional phase shift at the front facet for each beam corresponding to the optical path length of one round trip. The number of output beams is given by the number of round trips through the active layer before attenuation at one of the edges and therefore depends strongly on the input angle.

Recall that the active layer can be described as a Fabry-Perot cavity. Often, monochromators are constructed by using Fabry-Perot cavities with nearly normal incident beams. Here, the angle of incoming light is usually different from 0° and therefore the effects of interference which are dominant for the monochromator can be less important. In general the effects of interference depend on the input angle of the injected light. The consequences of using injected beams with different input angles and/or different beam sizes following from these considerations are best discussed directly in comparison with our experimental results. Therefore, we postpone that discussion until chapter 8.

Modeling the laser as a Fabry-Perot cavity has been shown to predict all experimental results. In the paper by Abbas *et al.*, [2] this model is reported to make additional predictions about the near and far field of the outgoing amplified beam which are quite consistent with experimental results. With

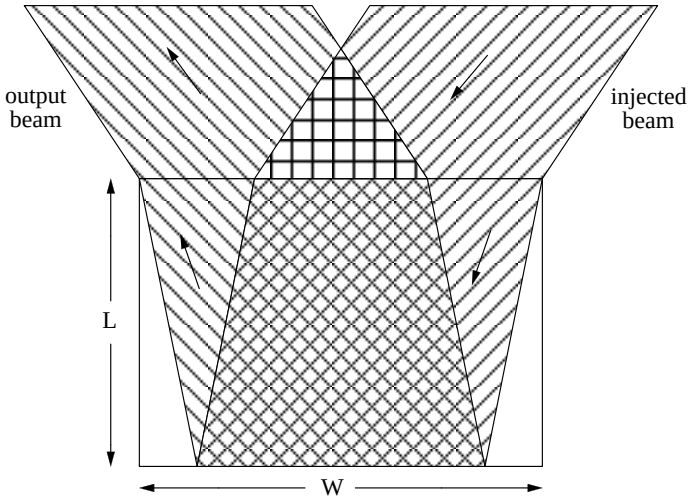

Figure 4.2: Ideal double-pass amplification, the front facet is effectively non-reflecting and the beam is reflected only once, on the back facet of the diode. The effects of interference between the beams are negligible.

our experimental setup and the measurement methods we had at hand (see chapter 6) we were unfortunately not able to verify these predictions.

Let us now discuss one limit of the model in which it becomes even simpler. If the front reflectivity is extremely low, as for example in highly anti-reflection coated diodes, the gain factor is very high. In this case, even a small injected light intensity is amplified on a short path and becomes comparable to the stationary intensity of the free running modes. At this point the injected light starts to have a significant impact on the population inversion. The inversion is lowered until the pumping process is again able to balance the stimulated emissions induced by the injected light. Although the injected intensity can be amplified by a large factor during its first round trip, the assumption that each following round trip produces another Gaussian output beam with the same intensity is no longer true. The product of gain and

reflectivity can drop so much below unity that the beam reflected back into the active layer is negligible compared to the input light. That means that the front facet just becomes effectively transparent and the outgoing light is structured as shown in Fig. 4.2. The effect of the active medium is basically reduced to that of a double-passed amplifier. Because of the large gain during the first round trip this regime can be effective. Unfortunately, we were not able to work in this regime with our components. One possible explanation is that our diode's front reflectivity is too high (§8.3) and therefore the gain per round trip small.

Chapter 5

The Experiment

Now that we have discussed the theoretical background described in Chapters 2, 3 and 4, we will describe the experiment. We will start by giving an overview of the setup in Section 5.1 and a description of the alignment procedures in Section 5.2. We continue with the possibilities of improving the amplification efficiency in Section 5.3 and then give a more detailed picture of some of the equipment used in Section 5.4. Because of their importance, the two lasers are discussed separately in Chapter 7.

5.1 Setup

Our setup is designed to guide the beam of the single-mode master laser (Section 7.1) into the active layer of the broad-area slave laser (Section 7.2). We measure the behavior of this diode (i.e., the characteristics of the outgoing light) in order to observe and investigate injection locking. In the following description let the master laser's beam be our guide through the setup shown in Fig. 5.1.

In controlling a beam, lenses are usually used to vary the beam width, and mirrors are used to direct it spatially. In order to have full control over

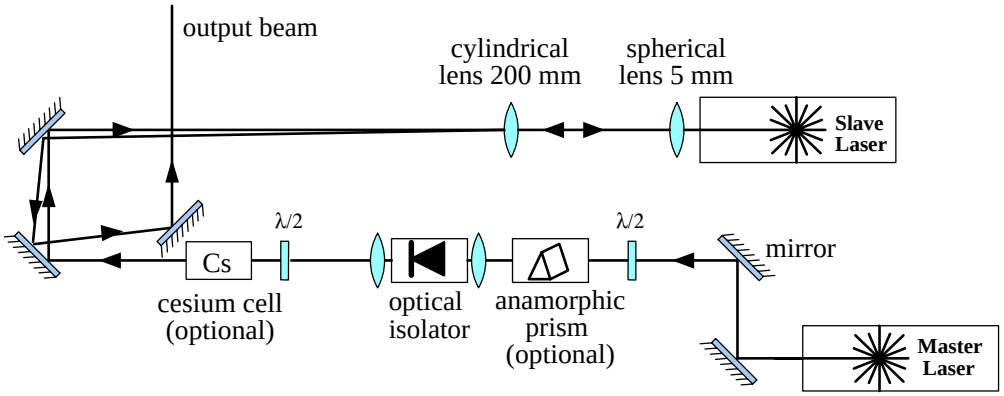

Figure 5.1: Experimental setup. The distances and angles are not to scale. The beam of the free running slave laser is omitted for clarity.

the direction and the location of a laser beam one uses the mirrors in pairs, such that one of them is used to control the beam position on the other mirror that itself directs the beam into the desired direction.

The first two mirrors in front of the master laser are an example of this technique and give us control over the beam that leaves the master laser in a fixed direction. When the wavelength of the master is changed this direction varies and one must adjust these mirrors to compensate.

Optionally, an anamorphic prism pair, as described in Section 5.4.2, is included in order to change the spatial beam characteristics of the master laser. Because the prisms have uncoated surfaces at Brewster's angle, a $\frac{\lambda}{2}$-plate is included to change the polarization of the light appropriately when the prism pair is included.

The next crucial component that the beam passes through is an optical isolator that works, in essence, like a diode in electronics but for light (see

Section 5.4.3 for a detailed description). It protects the master laser from feedback. In other words, it prohibits light from the slave laser or back-reflected light from the master itself from entering the diode's resonator. The master laser is extremely sensitive to feedback, which makes the optical isolator absolutely necessary. A lens with 100 mm focal length is used to focus the beam onto the front of the isolator because of its small aperture. To recollimate the beam behind the isolator, one can use another lens with the same focal length. However, using different lenses allows us to use the isolator setup simultaneously as a beam expander to vary the beam width. A second half-wave plate is included to match the polarization from the isolator to that of the slave laser, as shown in Fig. 5.1.

The cesium vapor cell is another optional component. We only use it to tune the master laser to the cesium D_2 line at 852 nm, which is the wavelength we plan to use in the long run. The cell can also be used to restore this fixed point in frequency when no frequency resolving measurement is available (see Section 7.1). As the name suggests, it is a glass cell that contains cesium in the gas phase that lights up due to resonance fluorescence whenever the incoming beam has a frequency within the Doppler-broadened linewidth of the D_2 line.

The two mirrors on the left allow another independent adjustment of the beam position and direction and deflect the beam towards the slave laser. To overcome the limited length of our optical table we sometimes included several more mirrors in order to vary the available path length of the beam between the second half-wave plate and the cylindrical lens (see below).

Let us discuss the coupling process of injecting light of the master into

the slave's active layer. The most critical parts of the beam path are a 200 mm focal length cylindrical lens and a 5 mm focal length spherical lens directly in front of the slave laser. The cylindrical lens is set up such that it focuses down light in the horizontal direction and does not affect it in the vertical direction. Therefore, in the vertical direction the beam is focused down solely by the 5 mm lens. Alignment of the cylindrical lens can vary the horizontal width, divergence and position of the master laser's beam at the active layer of the broad area diode (see Section 5.2 for details). This lens is mounted on a two-dimensional translation stage for ease of alignment.

The spherical lens, model #1403-.108 from Rodenstock Precision Optics, Inc., is mounted on a three-dimensional translation stage. Its focal length is small because it also serves to collimate the slave laser's beam, which is diverging rapidly, into a roughly collimated beam in its vertical direction. Another advantage of such a small focal length is that one can focus down the master's beam very tightly in order to produce very small beam widths near the focal plane. This is one step that is necessary in order to hit the thin active layer with as much power as possible. The aberration of the slave's beam (Section 7.2) results in horizontal divergence, even after collimating with the 5 mm lens, but can be partly compensated by the cylindrical lens if desired.

One has several options for analyzing the light outgoing from the injected slave laser. First, one can include a beamsplitter (not shown in Fig. 5.1) between the second half-wave plate and the cylindrical lens. Approximately 10% of the intensity reaching the beamsplitter from the slave laser's side can be coupled out for measurement without losing the ability to inject light into

the slave completely. Naturally, this option also implies that 10% of the master's intensity is lost for injection when it passes through the beam splitter from the other side. Another option is to investigate only light leaving the slave diode with a small angle relative to the main beam and pick up this light after it traveled far enough to separate the beams (see Fig. 5.1 and Section 5.3). The smaller the angle, the larger the needed path length, and for small enough angles the separation from the slave laser's beam becomes impractical (see Section 8.2).

Despite the disadvantages of the separation method, the alternative method of using a beamsplitter cannot be implemented in the final setup. A beam splitter with high transmission results in weak attenuation of the master laser's power and therefore leaves a high intensity available for amplification. However, the output beam is then weak since only a small amount of the amplified light is reflected out because of the small reflection coefficient. In contrast, if one uses a beamsplitter with a low transmission coefficient, only a small percentage of the master laser's intensity reaches the slave laser in the first place. Therefore, neither beamsplitter option is viable for any application that needs high power.

Using the separation method may not be as bad as it seems, even if the separation of the amplified beam from the others is imperfect. The amplified beam must be spatially filtered, regardless, to make sure that it is in a single spatial mode. This is usually done by putting a small aperture (50 μm) at the waist of the beam so that all modes except TEM_{00} are blocked. The beam input to the spatial filter must be focused with critical precision in order to

pass through such a small aperture. This critical alignment rejects any light that is only slightly diverging, including the excess slave laser light.

The spectrometer and the cavity used for the frequency-resolving measurements of the output beam are described in more detail in Sections 6.2 and 6.3. Other power measurements are done with standard commercial power meters based on photodiodes or the thermoelectric effect.

5.2 Alignment

There is one general drawback to working with 852 nm light: infrared light is invisible to the human eye. To handle this problem there are fluorescent cards that show a bright spot when inserted in the beam and handhold infrared viewers that use a cathode-ray tube. The cards are not always useful because of their limited sensitivity and because they have to be physically inserted into the beam and therefore block it. From this point of view, the viewer is more comfortable but unlike the human eye it is not auto-focusing.

The discussion of alignment will again start at the master laser. Here, we assume that the master laser is properly aligned. We will come back to this point in Section 7.1 where the master laser is discussed in detail.

The alignment of the beam through the optical isolator is straightforward. First one matches the horizontal polarization required by the anamorphic prism (if inserted) by turning the half-wave plate. For that purpose, one can remove the cover of the anamorphic prisms to observe the beam propagation through it more easily (see Section 5.4.2 for a detailed description of the prism). Because the light leaving the anamorphic prisms is still polar-

ized horizontally, the first of the isolator's polarizers has to be turned in this direction as well. The second one is placed at a relative angle of 45°. The orientation of both polarizers is optimized by minimizing the power losses in this part of the setup after the beam is directed through the prism and the isolator's aperture. The half-wave plate in front of the anamorphic prism is not removed even when the prism is, because otherwise the polarizers in the isolator must be completely realigned. All power measurements at this stage can be done by inserting a power meter directly into the beam path. To optimize the isolator further, one can direct light from another source, e.g. the slave laser, through the isolator from the opposite side such that it should stop the beam. By adjusting the polarizer on that back side to minimize the transmitted power, one can make sure that the isolator extinguishes as much light as possible without increasing the loss in the master beam. Aligning the isolator has to be done carefully because its strong magnetic field (Section 5.4) attracts screwdrivers and tools in general. Hitting the isolator can spoil the alignment, or even worse, damage the isolator itself.

The second half-wave plate rotates the polarization in order to match the vertical polarization of the slave laser beam, because only vertically polarized light can couple to the active medium in the slave diode (§7.2) and be amplified.

Before we discuss the alignment of the master laser's beam into the slave, we first discuss the alignment of the two lenses in front of the broad-area diode. The lenses' positions along the optical axis are most crucial for the injection of external light into the active layer of the slave laser. The quality of

the alignment cannot be judged before the master beam is actually hitting the active layer. It is helpful to begin with the lenses along the optical axis such that the slave beam is as collimated as possible. The collimating lenses should be placed such that the propagation is along the same axis as the uncollimated beam. This fixes the position of the two lenses in planes perpendicular to the beam. With this alignment the useful lens area is maximized, which is beneficial since the 5 mm focal length lens is only 4 mm in diameter and is therefore not much bigger than some of the beam widths. Clipping on the lens mount can lead to losses in the overall power of the final amplified beam. Nevertheless, lenses mounted perfectly perpendicular to the beam can increase feedback effects and should be avoided.

For effective amplification it is absolutely crucial to couple as much power as possible into the active layer. Therefore, a critical part of the alignment is to find the right beam path for the master laser which actually results in injecting the largest amount of power into the slave. Because the active layer of the slave laser is relatively tiny (200 μm $\times$ 3.5 μm) a rough alignment to start with is not enough and at the length scale of a few micrometers one cannot simply steer the beam visually. The measurement of the height of the active layer is described in Section 7.2 while the 200 μm width was given by the manufacturer.

Following a technique described by Praeger *et al.* [7], for example, it is therefore easiest to start the alignment procedure by overlapping the two beams (incoming master and outgoing slave laser) as well as possible. By symmetry, the master laser's beam retraces the slave beam right into the active

layer if the two beams' positions coincide at two different points in our setup. This can be achieved by an iterative process using the two mirrors shown on the left in Fig. 5.1. One alternately overlaps the beams at two chosen points by turning one of the mirrors for matching the beams at each point. Naturally, placing the two points further apart will improve the accuracy of the alignment. It is also helpful to operate the two lasers at similar output powers so that both beams are visible either with an infrared viewer or with a fluorescent card.

5.3 Separating the Amplified Beam and Increasing its Intensity

Having finished the discussion of the basic alignment we now proceed to the search for amplification. Typically after following this procedure, the alignment of the system turned out well enough to produce a measurable injection effect.

Usually the fraction of the intensity resulting from amplification of the master beam was not very large. To make improvements possible, one has to monitor the outgoing light either by inserting a beamsplitter as discussed in Section 5.1 and using a frequency-resolving measurement technique or by separating the part of the emitted power that consists of amplified master laser light from the rest of the output.

Separation can be achieved by shifting the cylindrical lens horizontally away from the optical axis by a small amount using one of the translation stages [7]. This results in a bending of the master laser beam when propagating

through this lens. Therefore, it will hit the active layer at a small non-zero angle. The part of the outgoing light resulting from amplification leaves the active layer at the same angle (see Fig. 4.1). When this amplified beam passes the spherical lens again it will propagate with a small angle ϕ relative to the incoming master laser beam. Ray tracing predicts $\phi = (0.57°/\text{mm})y$, where y is the transverse displacement of the lens. This prediction is in good agreement with our experiment.

Naturally, the excess slave laser light will also be bent and will no longer overlap the master beam (see Fig. 8.4). However, the angle between these two beams is smaller than ϕ. Therefore the injected, amplified, and reflected beam can now convert its angular separation into spatial separation by propagating some distance. It can be picked up after a sufficiently long beam path without blocking the injecting master laser beam, as shown in Fig. 5.1. At small input angles one reaches a regime where the divergence of the slave's beam (Section 7.2) is larger than the separation angle between the beams. At this point a full separation is no longer possible and frequency-resolving measurement methods have to be used.

Once the beam is picked up, the alignment for the different measurement methods is either straightforward (e.g., for the power meter) or discussed in Sections 6.2 and 6.3. There is a general drawback to our measurement methods, which is that every realignment of the master-slave system spoils the alignment used for that measurement. We have not been able to find a way to decouple these processes.

We are finally in a position to investigate the behavior of the broad-area

diode injected with light under different conditions. The positions of the lenses relative to each other and relative to the active layer together, with the initial width of the master beam determine the shape of the injected beam at the front facet. These factors control the efficiency of the injection as discussed earlier. The theoretical models for beam propagation (Sections 3.1, 3.2.2) can be used to predict these beam shapes. For comparison, the shapes can be measured by removing the slave laser and using the knife edge method (Section 6.1) at its usual position (Section 8.1).

All of our results are especially sensitive to the position of the 5 mm lens in the direction of beam propagation. This is understandable because the extremely short focal length implies that small changes in the lens position may lead to drastic changes in the width and the shape of the beams. The different possible alignments of the cylindrical lens relative to the spherical one are discussed along with the results in Section 8.1.

Small variations in the master beam direction, controlled by the mirrors used to overlap the beams, can be used to optimize the results. Another sensitive parameter is the input angle of the injected beam, which is controlled by the transverse displacement of the cylindrical lens (Section 8.2). Finally, one can optimize the injected intensity by slightly changing the polarization direction of the master laser. This is most easily accomplished by turning the second half-wave plate in the setup in order to minimize the difference between the two polarizations (Section 8.4).

There are other parameters besides the optical parameters that can be varied in order to investigate the system and find optimal settings. The driving

currents and temperatures of the two lasers also have major impacts on the injection behavior. First of all, different slave settings result in different center frequencies and, more importantly, in different cavity lengths. Furthermore, variations in the driving current or the temperature of the master can slightly change the wavelength of its emitted light. The results with different driving currents and temperatures are discussed in detail in Section 8.3.

5.4 Setup Components

In this section we will discuss the components that are used in the setup in more detail. Since the lasers are of special importance they are discussed separately in Chapter 7.

5.4.1 Half-Wave Plate

Half-wave plates are used to rotate the direction of polarization of linearly polarized light. Waveplates in general are constructed from a uniaxial, birefringent material (such as quartz) cut such that the optical axis is parallel to the front and back surfaces. The components of the incident beam with polarization perpendicular (ordinary) and parallel (extraordinary) to the optical axis will then propagate in the same direction but with different velocities. This results in a relative optical path difference between the components given by

$$\Delta s = d(|n_{\mathrm{o}} - n_{\mathrm{e}}|), \tag{5.1}$$

where n_{o} and n_{e} denote the indices of refraction of the birefringent material for the o- and e-waves respectively and d the physical length of the plate.

The value of $n_o - n_e$ depends on the used material but one can always choose d such that

$$\Delta s = \frac{\lambda_0}{2}(2m + 1), \tag{5.2}$$

where m is an integer. This corresponds to a phase shift of $(2m + 1)\pi$, or in other words to a shift of half a wavelength of light. One can show that a half-wave plate rotates linearly polarized light with a polarization angle of θ relative to the optical axis of the wave plate by 2θ. Hence, it reflects the polarization direction across the optical axis. If one places the wave plate such that its optical axis points 45° from the vertical, it will turn vertically polarized light into horizontally polarized light and vice versa. For a more detailed description of birefringent materials and wave plates see, for example, [17].

The alignment of a half-wave plate is rather uncritical. One only has to make sure that the beam hits the plate almost perpendicularly. Imperfect alignment has the advantage that feedback effects into the laser are reduced.

5.4.2 Anamorphic Prism Pair

Anamorphic prism pairs are used to change the cross-sectional width of a laser beam in one direction while not affecting the other. In our application, we use it to decrease the horizontal width of the master beam. The anamorphic prism pair consists of two identical prisms mounted as shown in Fig. 5.2. The prisms are aligned such that the outgoing beam hits the surface of the prism under an angle close to the Brewster angle in order to allow propagation through the prism pair. This is why the prisms in our setup only work for

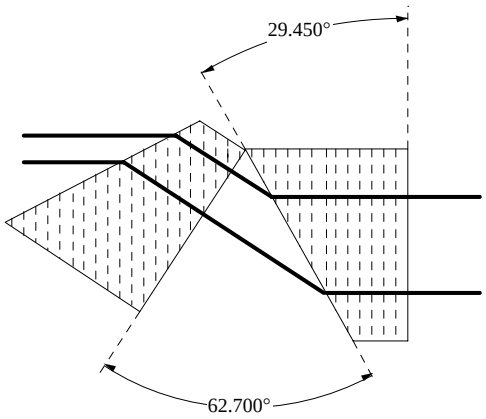

Figure 5.2: Anamorphic prism pair: In our case the beam enters from the right and leaves the prisms on the left

horizontally polarized light. As one can see in Fig. 5.2, the beam is not only compressed but also slightly shifted in the horizontal direction. The alignment of an anamorphic prism is described in detail in Section 5.2.

5.4.3 Optical Isolator

The optical isolator included in the setup prevents feedback into the master laser. It uses the Faraday effect, which describes the influence of a strong magnetic field on an optically active crystal (for a more detailed description of this effect see [18]). If the magnetic field is parallel to the direction of light propagation the medium becomes optically active in the sense that it rotates the polarization by an angle θ. It turns out that $\theta = VBd$ where B is the magnetic field, d the thickness of the medium and V is the Verdet constant that depends upon the material chosen and the wavelength used.

To build an isolator using this effect, one places the crystal between

two polarizers. The polarizer facing the input beam is oriented parallel to the polarization of that beam and the second at 45 ° with respect to the first polarizer. The thickness of the crystal is chosen such that it rotates any beam by 45° in the direction towards the second polarizer. Therefore a beam entering the isolator from the input direction passes unaffected through the isolator. However, a beam from the other side is polarized at 45° after the polarizer and is then rotated by another 45° in the crystal such that its polarization becomes perpendicular to the polarizer at the input. Most of the light is then rejected by this polarizer. The isolator we used is model IO-3C-852-VLP from Optics for Research and is specified at 37 to 42 dB of isolation. The alignment of the isolator is described in Section 5.2.

Chapter 6

Measurement Methods

This chapter is intended to introduce the methods we use to obtain information about the characteristics of our beams. The two main features of a beam are its shape and its spectrum. In Section 6.1 we introduce the knife-edge method used to characterize the beam shape. In Sections 6.2 and 6.3 we describe the measurement techniques to obtain spectral information.

6.1 Knife-Edge Method

In Chapter 3.1 we introduced the possibility of calculating the width of a beam. Naturally, any calculation needs an initial value of the beam width. Measuring the beam width is therefore a necessity even in cases where it can be calculated. One can also verify that the beams are Gaussian by comparing the measurement to the calculation.

In our setup the horizontal and vertical beam widths are obtained only indirectly by partly inserting a razor blade in the beam. One then measures the remaining (non-blocked) intensity at different blade positions (see Fig. 6.1). We used several translation stages to change the position of the blade in all directions. Assuming that the beam is Gaussian, one can then perform a

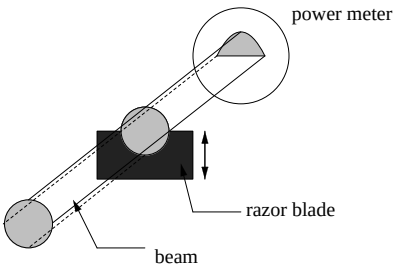

Figure 6.1: Knife-edge method: The position of the razor blade can be changed with a translation stage and the power in the remaining beam is measured.

least-squares fit of the measured intensities to the integral over a Gaussian intensity distribution (error function). We used the radius of the Gaussian distribution (Section 3.2.1), its amplitude, the center of the distribution and an overall offset as free parameters to fit the experimental data. The center of the Gaussian and the amplitude are not measured directly and are therefore included as fitting parameters. The overall offset parameter is included to account for stray light entering the power meter. Finally, the beam radius yielded by the fitted distribution is the parameter that we are interested in. Fig. 6.2 shows an example of such a fit and the corresponding Gaussian profile. By performing two separate measurements this technique provides us with the waist in both horizontal and vertical directions at one point in the beam path.

The knife-edge method yields a good estimate for the beam width. However, the disadvantage of the knife-edge method is that it is indirect and time consuming. It would have been easier to use a CCD to monitor the beamshape directly, but unfortunately we did not have one at hand.

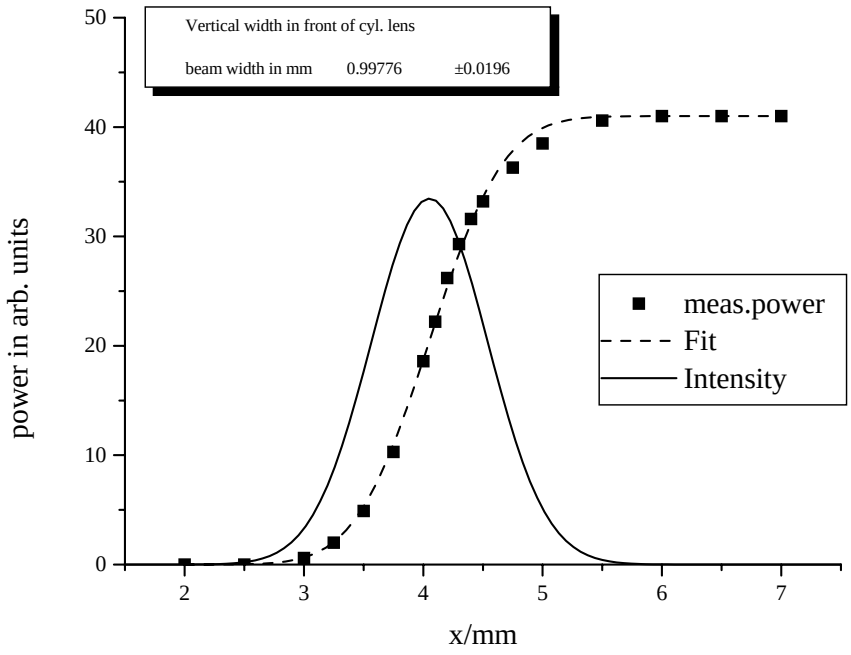

Figure 6.2: Example for the fit of the measured data to an error function and the corresponding Gaussian beam.

6.2 Spectrometer

We used a Czerny-Turner type monochromator to get high resolution, gauged spectra. A schematic drawing of the spectrometer is shown in Fig. 6.3. It contains an adjustable slit for the incoming beam, several mirrors to guide the beam within the device and another slit for the outgoing beam. The heart of the spectrometer is a blazed diffraction grating that can be rotated with different velocities by a step motor.

A close-up of the grating is shown in Fig. 6.4. The goal is to obtain the maximum intensity in the first order of the diffraction pattern. To achieve

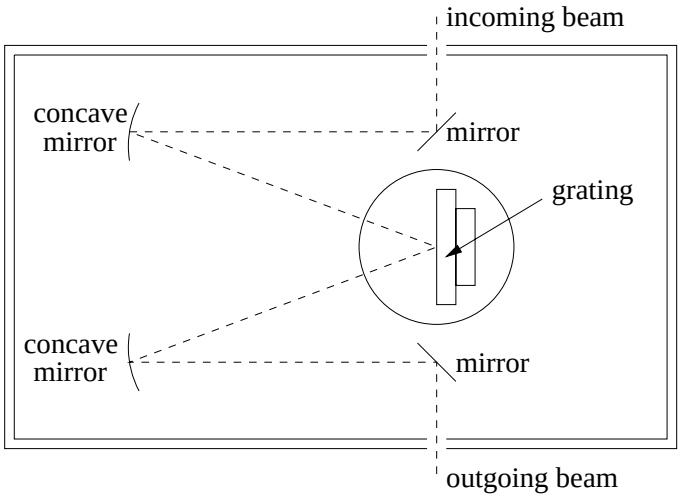

Figure 6.3: Schematic of our spectrometer: The dashed line shows the beam path.

this goal, the angle for reflection α, the angles for constructive interference θ_{in} and θ_{out} and the angle β of the grating must satisfy the relations

$$\begin{aligned} \theta_{\text{in}} &= \alpha - \beta \\ \theta_{\text{out}} &= \alpha + \beta. \end{aligned} \tag{6.1}$$

For a given θ_{in} one can obtain θ_{out} using the Bragg condition for an intensity maximum in the diffraction pattern of a grating

$$b(\sin\theta_{\text{out}} - \sin\theta_{\text{in}}) = 2\pi\lambda, \tag{6.2}$$

where b is the periodicity of the grating and λ is the wavelength[1]. Equations 6.2 and 6.1 together yield the condition for the wavelength λ that has an intensity maximum in the first order,

$$\lambda = \frac{d\sin\beta}{\pi}\cos\alpha. \tag{6.3}$$

[1]See for example problem 12 on page 925 of Tipler [20].

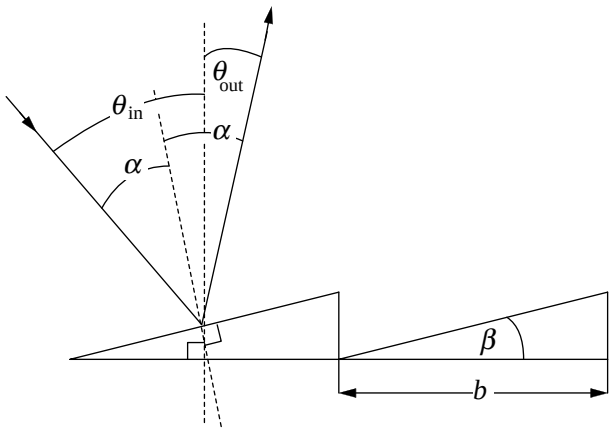

Figure 6.4: Diffraction grating: Note that the normal axis for reflection and diffraction (dashed lines) are different. Equation 6.3 can be easily extracted from the geometry shown.

The spectrometer is designed such that only this specific wavelength gets scattered in the right direction to pass through the second slit. One must align the spectrometer such that the beam enters roughly perpendicularly to the slit in order to get a beam path as shown in Fig. 6.3. The concave mirrors make this alignment easier. The resolution of the spectrometer is determined by the width of the slit for the incoming beam and increases with decreasing width. However, one cannot make this slit arbitrarily small since reducing the slit width reduces the input intensity and therefore the signal to noise ratio. The finest resolution that the monochromator is capable of is about 15 GHz and the widest scan possible is hundreds of nanometers. The power in the outgoing beam is detected with a photomultiplier tube that is read by a Hewlett-Packard Plotting Measurement System. All the spectra shown in this thesis were drawn with this plotter. The main advantage of the spectrometer is that one gets a wavelength-calibrated output. Although

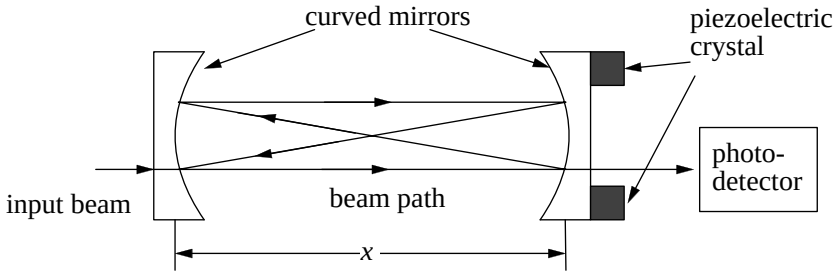

Figure 6.5: Schematic of a confocal Fabry-Perot cavity: The light propagates through the cavity four times per round trip. A photo diode measures the wavelength-dependent transmission.

the relative calibration (difference between two wavelengths) was reasonable the absolute offset was off by several nanometers. We usually determined this offset using the cesium line at 852 nm. Since the spectrometer has a variable resolution we were able to adjust it to our needs and resolve even widely separated spectra of the slave and the master laser in one picture. A drawback of this method is the long time (up to several minutes) needed for obtaining a single spectrum. Therefore, it is not suitable for resolving fast fluctuations of the system (i.e., its dynamical properties). Scanning a large parameter set for investigating injection locking (see Section 8.3) also is very tedious and practically impossible.

6.3 Confocal Fabry-Perot Cavity

The dynamical aspects of the spectra can only be visualized by using a scanning confocal Fabry-Perot cavity (see Fig. 6.5). A beam entering the cavity parallel to its axis of symmetry describes a closed path with an optical path length of $\Delta s = 4x$ per round trip where x denotes the distance between the two

curved mirrors which is twice the radius of curvature of each mirror. Since alignment is never perfect, the beam will enter the cavity at a small angle. One can show that the path is still closed in this case and that Δs is slightly larger than $4x$. To explain the principle of a Fabry-Perot cavity it is sufficient to notice that the path difference after each round trip of about $4x$ leads to constructive and destructive interference for different wavelengths. From the Airy-formulas [19] one gets a transmitted intensity

$$I = I_0 \frac{T^2}{(1-R)^2 + 4R\sin^2(\pi \Delta s/\lambda)}. \tag{6.4}$$

Here, T and R are the transmission and reflection coefficients of the cavity (the product of the corresponding coefficients of the mirrors) and I_0 is the incident intensity. For our cavity, R is about 0.99 which gives a value of 0.01 for T if we neglect absorption effects. One can calculate that I is rapidly varying with wavelength. Any $\lambda_0 = \frac{\Delta s}{m}$ (where m is usually of the order of 10^5) results in the maximum transmitted intensity $I = I_0$. The wavelength difference between two maxima is therefore

$$\Delta\lambda = \lambda_1 - \lambda_2 = \frac{\Delta s}{m(m+1)}, \tag{6.5}$$

where $\Delta s \approx 4x \approx 20$ cm for our cavity. Therefore, $\Delta\lambda$ is about 10^{-12} m, corresponding to about 1.5 GHz frequency difference between two adjacent maxima.

The Fabry-Perot cavity becomes a useful spectrometer if one uses a piezoelectric crystal to change the position of one of the cavity mirrors. This changes Δs and therefore the wavelength of the peak of the transmitted intensity. The piezo voltage can be swept at up to 10 Hz. We obtain an instantaneous spectrum every 0.1 seconds by measuring the light intensity behind

the cavity with a photodiode and monitoring it on an oscilloscope. We usually sweep the mirror a distance corresponding to roughly 6 GHz frequency difference for the peak at the same m. Therefore, each line appears 3-4 times because it also satisfies $\lambda_0 = \frac{\Delta s}{m}$ for different values of m every 1.5 GHz.

The cavity resolution of 4.8 MHz is incredibly high compared with that of the grating spectrometer. If the width of the incoming spectrum is narrow compared to the free spectral range of the cavity (1.5 GHz), the cavity works like a monochromator in that it only transmits a single frequency. However, for broad lines there will always be some wavelengths within the line that fulfill the condition $\frac{\Delta s}{\lambda} = m$ (for some m) and therefore one cannot resolve that line. A signature of this effect is an overall offset on the monitoring photodiode.

The main drawbacks of using the Fabry-Perot cavity are that the lines of the slave laser are so broad such that its spectrum cannot be visualized at all. It also is much harder to identify a certain peak with a frequency or wavelength, because the condition for a high transmission-coefficient is periodic. Nevertheless, the Fabry-Perot cavity has the important advantage that it produces *in situ* spectra (10 spectra per second). Any change in the spectra becomes immediately visible (for example when aligning the setup). In particular, for investigating large parameter ranges, the dynamical behavior of the laser system or feedback effects, this measurement method is invaluable.

Chapter 7

The Diode Lasers

Before investigating the physics of amplification of injected light, it is essential to obtain information about the free-running behavior of the laser components. This chapter is devoted to the discussion of the characteristics of the two lasers used in our experimental setup.

7.1 Master Laser

The master laser is a grating-stabilized, external-cavity diode laser. The laser diode itself is model SDL-5421-G1 from SDL, Inc. It is specified to produce 150 mW of cw light at 849 nm and is packaged in a standard 9 mm metal can. It is driven by a Newport model 505 laser diode driver. This driver is stabilized, but the output light still shows a ripple of up to 0.3% in power at 60 Hz as one can see on a scope measuring the output of a photodiode. The output current can be swept by applying an external control signal to the power supply. We stabilize the diode temperature at (29.9±0.1) °C with a Newport model 325 temperature controller connected to a thermoelectric cooler. The temperature is reasonably stable except when the ambient temperature fluctuates. For example, when our labmates baked out a chamber in

the same room as our laser, the laser temperature unlocked from time to time, and it took the controller some minutes to restabilize.

The threshold current of this laser varies slightly around 15 mA, depending on how well the external cavity is aligned in the vertical direction (see below). The output wavelength of the diode is specified to be 849 nm at room temperature, but it is usually possible to operate such a diode at 10 nm above or below that value. Because we mainly use the diode at 852 nm we choose the temperature of 29.9 °C (slightly above room temperature) in order to increase the power output at the desired wavelength (see Section 7.2 for more about the temperature dependence of diodes). At approximately 842 nm, the output power is reduced to half its overall maximum value.

The SDL-5421-G1 is a narrow stripe diode as described in Section 4.1. Therefore, its output intensity is limited to about 100 mW corresponding to a driving current of 200 mA. For safety reasons we operate the system up to an output power of approximately 90 mW, corresponding to 190 mA of driving current. At driving currents greater than 200 mA the lifetime of the laser is drastically reduced. Because of the narrow band structure, the master laser should lase in a single spatial mode, and the emitted beam should have the Gaussian intensity profile of a TEM_{00} mode. This expectation is in good agreement with our experimental result using the knife-edge method (see Fig. 6.2). Unfortunately, the beam produced by the diode is slightly astigmatic, and therefore the horizontal and vertical beam widths are not the same (see below).

The diode is mounted in a special setup [21] shown in Fig. 7.1, that pro-

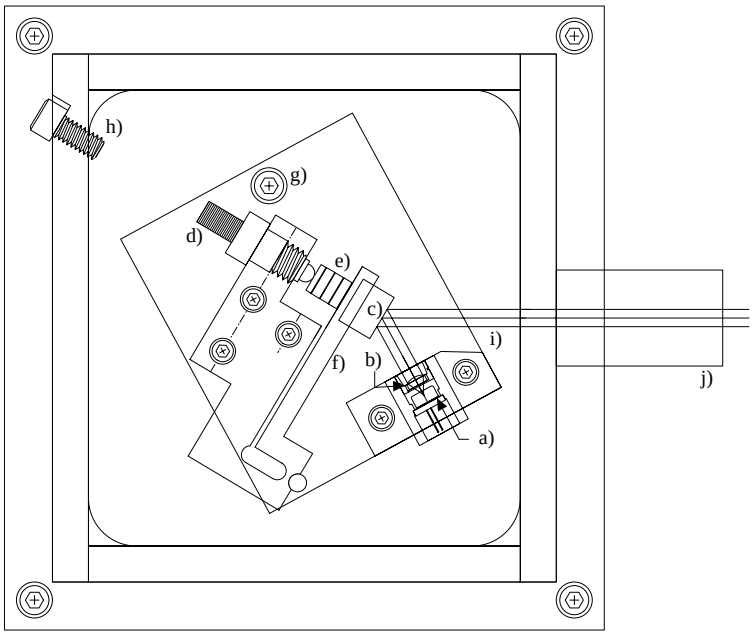

Figure 7.1: Design of the master laser: a) laser diode, b) collimating lens, c) diffraction grating, d) screw for wavelength adjustment (for turning the grating), e) piezoelectric crystal for fine wavelength adjustment, f) aluminum bronze flexture arm, g) screw for adjusting the vertical alignment of the grating, h) housing hole for screwdriver access, i) outgoing laser beam, j) window at Brewster angle.

vides longitudinal single mode characteristics and furthermore tunable wavelength. Directly in front of the diode is a 5 mm focal length lens for collimating the laser beam. Because of the diode's narrow stripe structure, there should be no large astigmatism in the beam because the horizontal and vertical width of the active layer are comparable (see also Section 7.2). A single lens should then be sufficient to collimate the beam nearly completely. Nevertheless, our measurements show that the beam is fairly astigmatic. Just after it leaves the master laser system, the horizontal spot size is (1.6 ± 0.1) mm and shrinking throughout the setup, but the vertical size is (0.4 ± 0.05) mm and growing.

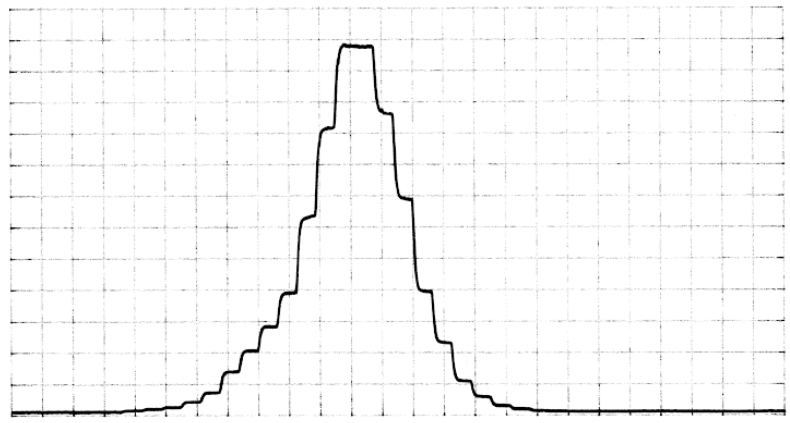

Figure 7.2: Master laser spectrum: the output is longitudinally single mode. The width of the peak is due to the resolution of the spectrometer and not related to the laser's linewidth. The individual steps are due to the step motor driving the spectrometer grating.

The diode front facet is antireflection coated, and the laser cavity consists of the highly reflective rear facet and an external diffraction grating. The grating is mounted in the Littrow configuration, where the light in the first order is diffracted back towards the diode. Only in a certain narrow wavelength band (depending on the angle of the grating) the light in the first diffraction order is reflected back into the diode itself. Since the amount of light reflected back by the grating is much larger than the amount of light reflected by the front facet, the external feedback dominates the behavior of the laser. In other words, the laser resonator is formed between the rear facet and the grating. Therefore, the laser can only oscillate within the narrow wavelength band (see Sections 2.1.1 and 2.1.2). Thus, the grating acts as a frequency selective, partially reflective mirror that allows lasing only in one longitudinal

mode. Typically diodes with an external grating produce single mode light with a width of less than 1 MHz, which is small enough to be monitored on our Fabry-Perot cavity.

To guarantee efficient feedback for high and stable output power, the grating must be aligned in the vertical direction. Following MacAdam *et al.* [21], this alignment is most easily accomplished by adjusting the vertical angle of the diffraction grating to minimize the threshold current. The threshold current appears as a sudden change in the output power's slope as a function of driving current. This is usually monitored while sweeping the current back and forth across the threshold.

The grating is mounted on a semirigid aluminum bronze flexture mount. Its angle can be horizontally adjusted either manually with a screw or with a piezoelectric crystal. The screw is accessible through a hole in the case (see Fig. 7.1), and one full turn corresponds to a wavelength shift of about 10 nm near the cesium line. Because a balldriver is used to turn the screw the precision is poor (10%). To avoid further accumulation of inaccuracies due to backlash, one can recalibrate the absolute wavelength using the cesium cell (see Section 5.1).

The output beam is the zeroth order of the grating and therefore changes direction whenever the grating is rotated. The angle variations are small but still large enough to miss the aperture of the optical isolator completely when changing the output wavelength by 5 nm (see Section 5.2). The laser output is vertically polarized, and a window at the Brewster angle is used to couple the light out of the housing without attenuation due to reflection

losses.

The small frequency interval in which lasing oscillations can build up is given by the grating position as described before. Within this interval the frequency of the lasing longitudinal mode can shift with changes in temperature or driving current. If this drift gets too large and another longitudinal mode enters the region of potential lasing, then mode hopping can occur, where the laser suddenly changes its output frequency. A similar effect can occur due to mechanical drifts in the grating alignment. The drifts of the grating are usually small (less then 10 MHz per minute) and can be observed with the Fabry-Perot cavity.

Our biggest problem in running this system is that it is extremely sensitive to external feedback. The optical isolator should prevent any back-reflecting, but in our setup the slave laser is shining directly at the isolator and even its large attenuation factor is not sufficient. Destabilization may be observed using the Fabry-Perot cavity. On a time scale of about 10 minutes stable operation may be interrupted several times by mode hopping or lasing on two different longitudinal modes when the slave laser is running. A slight tuning of the master diode's driving current is sufficient to restore stable operation in most cases. Apart from these minor problems, the master diode works reliably and proves to be perfectly suitable as a single-mode light source to be injected into the broad-area diode.

7.2 Slave Laser

So far, we have described the characteristics of the master laser used in the experiment as a stable single-mode light source. However, we are more interested in the characteristics of the free-running slave diode. Because it is the heart of our experimental setup, understanding its free-running behavior is a crucial step in understanding and judging the effects of the injected beam.

The slave laser is a Polaroid POL-5200-E TO-3 series high power diode laser. It is packaged in a TO-3 can with an anti-reflection coated sapphire window, a thermoelectric cooler and a thermistor. The diode is specified to have an output power of 2 W which occurs (according to Polaroid test data) at a driving current of about 2.67 A. These high values are achieved as discussed earlier (in Section 4.1) by not restricting the active area of the diode. The diode puts out light through the approximately 200 μm wide stripe of the front facet, sacrificing the single-mode spatial structure of the emitted beam. The threshold current at room temperature is (400 ± 20) mA and increases with temperature to (450 ± 20) mA at 50 °C. The diode driver is a Wavelength Electronics LFI-3525, 3.25 A current supply. The temperature is regulated by a Wavelength Electronics LFI-4532 temperature controller. The feedback to the controller is read from the thermistor in the diode can. A table to convert the thermistor value shown on the controller's display into temperature in degrees Celsius is given in Appendix B.

The collimation of the slave laser light into a beam was discussed in Section 5.2. At 1 A driving current the beam widths after propagating through the lens system are (2.1 ± 0.1) mm vertically and (2.5 ± 0.1) mm horizontally,

as measured with a knife edge. The fits to the error function do not show the multi-mode spatial structure of the beam in a significant way and seem to be quite useful to extract the beam width. Because of the wide active area and its small height, the beam starting from the front facet should be very divergent in the vertical direction and less so in the horizontal direction. That leads to an astigmatism in the beam that cannot be completely overcome even with the cylindrical lens included in the setup. Therefore the beam width slowly increases while the beam propagates through the setup. This divergence leads to difficulties in separating the amplified part of the light from the free-running component (see Sections 5.3 and 8.2).

The coupling of master laser light into the slave's active medium is the most crucial step in an effective injection setup, so it is helpful to know the height of the active layer itself. We were told by a Polaroid representative that the height is about 1 μm although they did not have the exact figure. Using the knife-edge method (Section 6.1) it is possible to measure the beam width in the vertical direction. By measuring at several points close to the diode, where the diverging beam is still small enough to fit onto the power meter's surface we should be able to estimate the active layer's height. Fitting the results of those measurements to the predictions of Gaussian beam propagation (Section 3.2) with the initial vertical width at the diode's front facet as fitting parameter yields a good estimate for that height (see Fig. 7.3). The distance between the knife edge and the diode is hard to measure and therefore it must be included as a second fitting parameter. This method yields an overall width of (3.5 ± 0.2) μm, which is only three times the wavelength of the light. Therefore focusing down to such a small active layer becomes very hard (see Section 8.1).

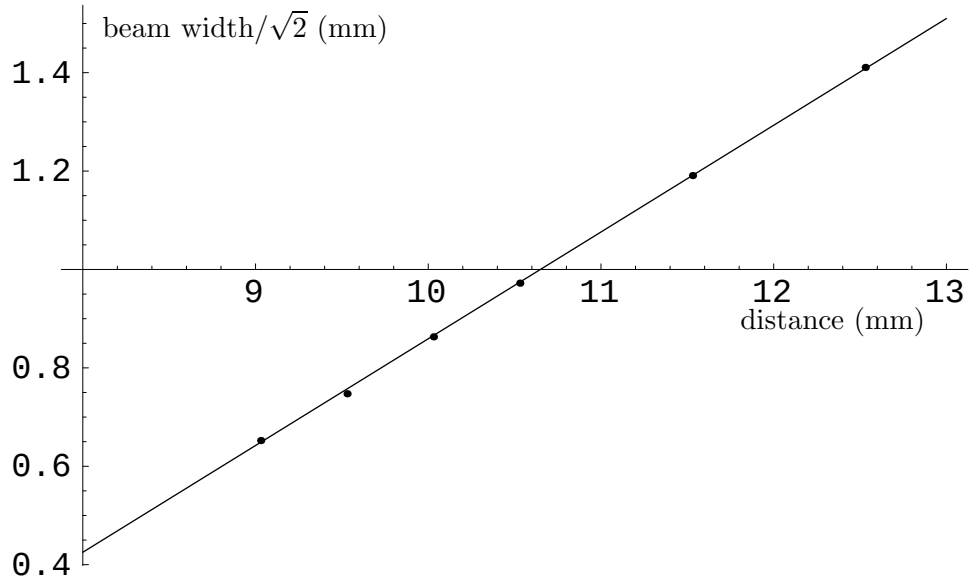

Figure 7.3: Measurement of active layer's width: the data is taken by the knife-edge method. The distance plotted is not the real distance from the front facet but (6.0 ± 0.5) mm larger (extracted from the fit). The resulting beam radius used to fit the solid line is (1.77 ± 0.10) mm. The plotted part of the diverging beam width is already in the asymptotically linear range (see Section 3.2).

The light emitted by the slave is linearly polarized in the direction perpendicular to the active layer because the pumped transitions emit only this polarization. Here, due to the orientation of the laser in our setup, the light is vertically polarized.

In contrast to the master laser, the broad-area diode is completely free running in the sense that no external cavity restricts its behavior. Therefore one can expect a longitudinally multimode structure. A spectrum taken with the grating spectrometer at room temperature (25 °C) and slightly above the threshold current is shown in Fig. 7.4.

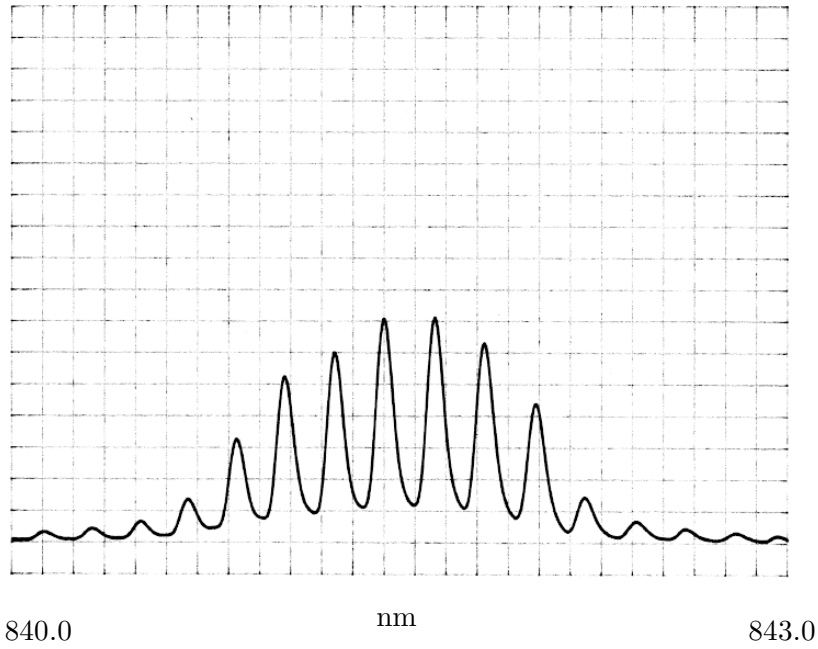

Figure 7.4: Slave laser spectrum measured at 25 °C and 0.41 A, slightly above threshold current. The spectrometer can easily resolve the different longitudinal modes.

From the distance in frequency and Equation (2.6), one can extract the length of the laser resonator, i.e. the distance between the two mirror like surfaces. The index of refraction of GaAs is $n = 3.64$, and the mean distance between longitudinal modes from Fig. 7.4 is (0.192 ± 0.005) nm (see [13]). The diode itself is made out of GaAlAs but the amount of aluminum does not greatly change the index of refraction since Δn scales like $-0.7(1 - i)$ where $1 - i$ is the percentage of aluminum (a number between zero and one) in the crystal (see Section 2.2.2). Therefore the cavity length can be estimated to be between 500 and 600 nanometers depending on the exact amount of aluminum in the diode, which we do not know.

The different amplitudes beautifully reflect the different stationary in-

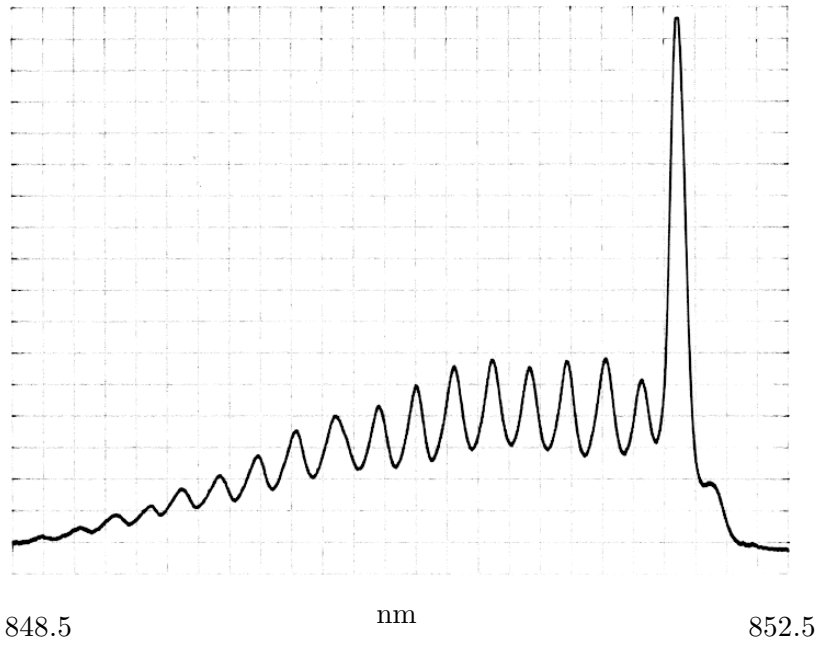

Figure 7.5: Spectrum of slave and master laser: The slave laser's current is 2 A, the temperature 45 °C. The two laser beams are entering the spectrometer separately (one through a beam splitter), so no injection of the master beam occurs. Due to the higher driving current more longitudinal modes are lasing than in Fig.7.4.

tensities inside the diode due to the frequency-dependent gain, as discussed in Section 2.2. Because of the limited resolution of the spectrometer the linewidths seen in the spectrum seem to be again much broader than they really are. Nevertheless, the spectrum is too broad to leave a visible signature in the spectrum taken with the Fabry-Perot (see Section 6.3). The slave laser light only increases the background level of any spectrum taken with the Fabry-Perot cavity. Only the grating spectrometer, with its drawbacks, can then be used to gain information about the changes in the spectrum of the slave while injected with master laser light.

The slave laser spectrum shifts with temperature and driving current as

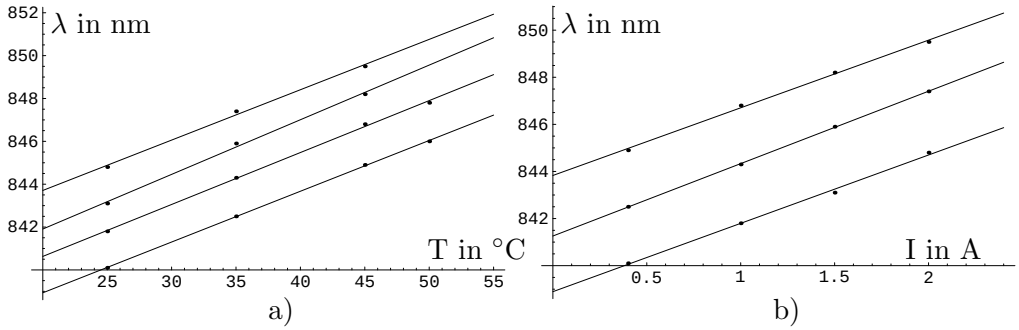

Figure 7.6: Center wavelength of slave laser: a) as a function of temperature at different driving currents, b) as a function of driving current at different temperatures

expected. For example, at a temperature of 45 °C and the maximum driving current of 2 A, the spectrum is centered at roughly 850 nm (see Fig. 7.5). It turns out that the center of the spectrum (peak of highest intensity) increases linearly both with temperature and with driving current as shown in Fig. 7.6. The proportionality constants are (0.245±0.010) nm/°C for temperature and (2.95±0.10) nm/A for driving current. The cavity length does not change significantly with temperature or driving current, but the gain curve clearly changes with driving current as can be easily seen by comparing Figs. 7.4 and 7.5 and as is expected from the discussion in Section 2.2.1.

In the free-running spectrum of the broad area diode, the effects of feedback also reveal themselves in a beautiful way. Figure 7.7 shows the spectrum of the slave laser with and without feedback. The feedback in this case is due to the second quarter-wave plate in the setup reflecting a tiny part of the intensity back to the slave. An undisturbed spectrum like that in Fig. 7.4 can be restored by blocking the quarter-wave plate with a simple piece of paper. As opposed to the multi-pass amplification experiment no light is intentionally

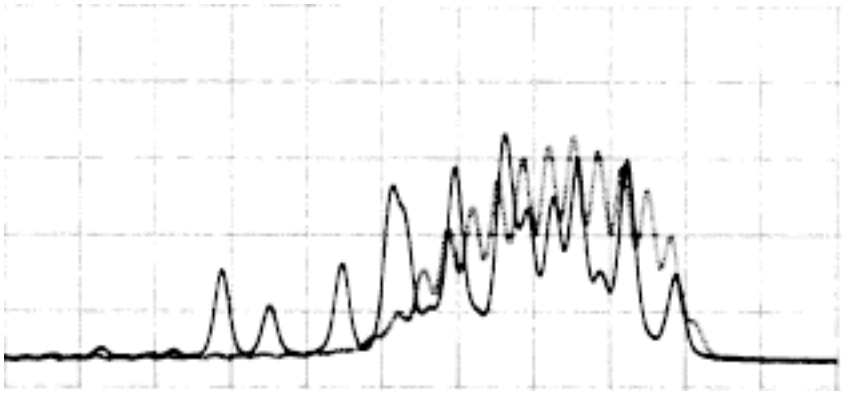

Figure 7.7: The effect of feedback: The light line shows the spectrum without feedback as in Fig. 7.4. The dark line is the spectrum disturbed by light back-reflected into the slave active layer.

inserted into the active layer in this case.

Chapter 8

Results

After presenting the theoretical background and our experimental setup and measurement methods, we are now able to discuss the behavior of our injected slave diode. We present our results by looking at the effects of the various parameters in our experiment. The effects of different alignment and beam parameters, positions of the cylindrical lens, driving currents of both lasers, slave laser temperature, and polarization are discussed in the following sections. This chapter concludes with a discussion of the dynamical behavior of the laser system.

8.1 Alignment and Beam Parameters

In general, aligning the setup as described in sections 5.2 and 5.3 is sufficient to produce some amplification. We now discuss how alignment affects the experimental results in greater detail and describe the most important ways to improve the amplification efficiency.

One critical part of the optical alignment of is the position of the spherical lens in front of the broad-area diode. The slave laser's front facet needs to coincide with the focal plane of this lens in order to ensure collimation of

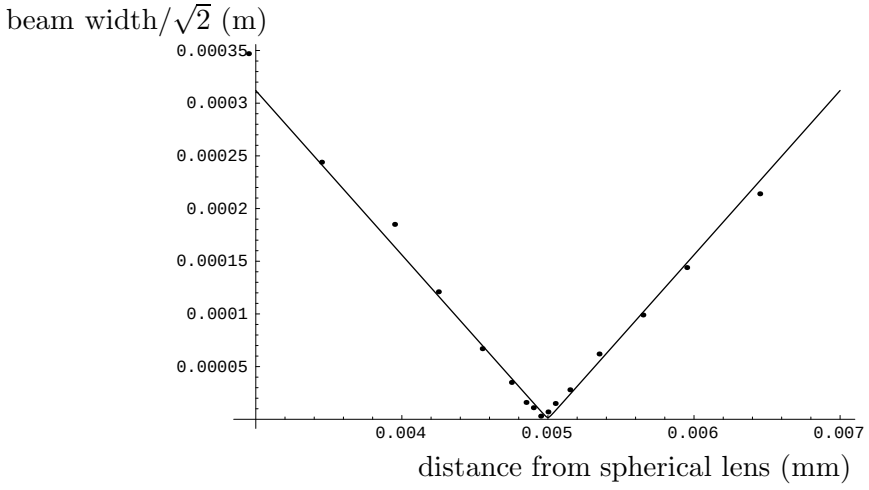

Figure 8.1: Vertical beam radius after spherical lens: The beam is tightly focused in the vertical direction. To determine the minimum beam waist, we fit a curve according to Gaussian beam propagation to our data points. This results in a minimum beam radius of (7±1) μm.

the outgoing slave beam. More importantly, this is also necessary for efficient focusing of the master's input beam onto the active layer. Since we measured the active layer to be only 3.5 μm thick, this presents a technical challenge. Naturally, only light that actually hits the active layer can be coupled into it.

According to Gaussian beam propagation, the beam radius at the focal plane is strongly dependent on the initial radius. The larger the incoming beam, the better it can be focused. Roughly doubling the beam radius in the vertical direction from (0.9±0.1) mm to (1.7±0.1) mm in front of the lens improves the overall amplification behavior by a factor of approximately four. Enlarging the beam further is unfortunately not possible because of the small aperture of the spherical lens, 4 mm. Figure 8.1 shows how we use the knife-edge method to extract the vertical beam radius in the focal plane of the spherical lens. With optimal beam parameters we can reach a total width of

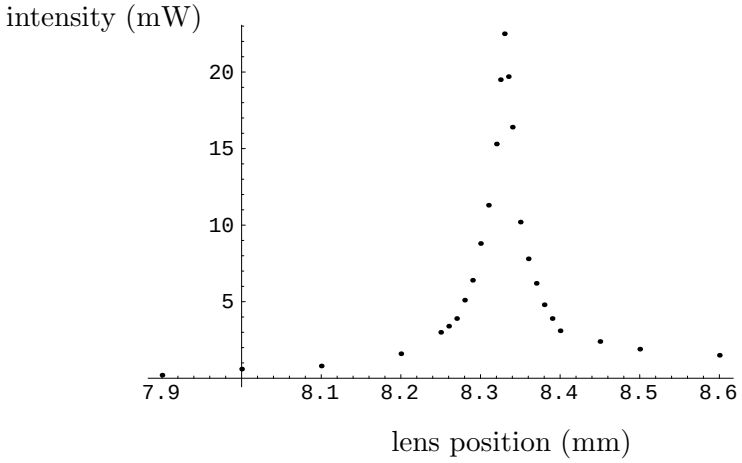

Figure 8.2: Intensity in the amplified beam versus position of the spherical lens along the direction of beam propagation: There is a sharp peak in the intensity. The absolute distance given on the position axis is shifted by an unknown offset. The peak indicates where the focal plane of the lens coincides with the front facet.

(7±1) μm which is comparable to the width of the active layer.

Naturally, shifting the spherical lens in the direction of beam propagation, i.e., shifting the focal plane around the diode's front facet, results in a rapid variation of the intensity coupled into the active medium. This is especially true because the minimum spot size is still larger than the thickness of the active layer. We have no way to determine the absolute value of the intensity coupled into the active layer, but the power in the amplified mode can reveal the relative efficiency of the coupling process. Figure 8.2 shows the variation in intensity in the amplified beam versus the position of the spherical lens. The curve is sharply peaked and the spatial resolution of the stage used to move the lens is not high enough to resolve the central part. This is one detail that seriously limits the efficiency of our setup. Additionally, slow drifts in the translation stage position lead to stability problems (see Section 8.5).

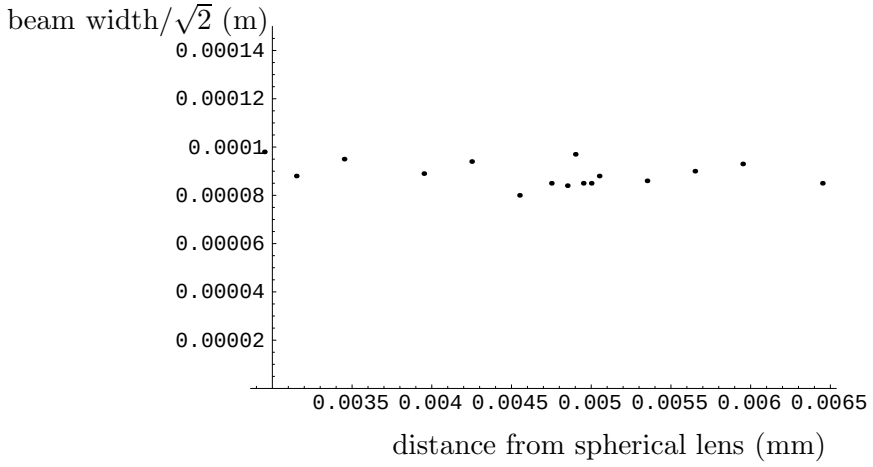

Figure 8.3: Horizontal beam width after spherical lens when the focal points of the spherical and cylindrical lens coincide: The beam is collimated in this direction.

Surprisingly, the technique of overlapping the beams before looking for any amplification works well. Changing the beam's position by turning one of the mirrors while monitoring the power in the amplified beam leads to only minor improvements.

There are in general two distinct ways to align the cylindrical and spherical lenses relative to each other. The first one is to try to collimate the slave laser beam as well as possible. The second is to overlap the focal points of the two lenses. Overlapping focal points mean that the master laser's beam is almost collimated, i.e., non-diverging, in the horizontal direction when it hits the active layer of the slave laser. This is the alignment that is most similar to the situation described by our theoretical analysis in Section 4.2. Figure 8.3 shows how well the beam can be collimated in this alignment. Despite the fact that the shapes of the outgoing beams change visibly we do not find a

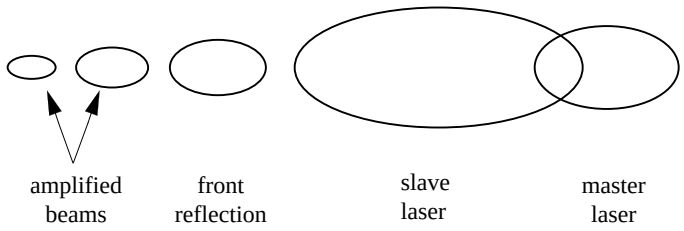

Figure 8.4: Amplification with large lens shift as seen with an IR viewer on a screen: The beam spots are clearly distinguishable. The master laser and the front reflection are visible even without running the slave diode. The beams of interest are those amplified by the slave laser. They disappear whenever either the slave or the master is turned off.

significant difference in the efficiency of the amplification process.

Another variable is the horizontal width of the injected beam when it is collimated at the active layer. From Fig. 8.3, we can extract a width of (127±5) μm. Inserting the anamorphic prism pair reduces it approximately by a factor of two. However, this does not lead to any major changes in the amplification behavior. It is possible to use nonspherical optics for more efficient matching of the injected mode to the active layer. Unfortunately, we did not have easy access to these components at the time of the measurements.

The experimental data and results shown in the following sections were taken at beam parameters and alignment that were as close as possible to optimal.

8.2 Input Angle

The input angle, as discussed in section 5.3, is determined by the transverse position of the cylindrical lens. A large separation angle between the incoming

and outgoing beams is easiest to handle because in this case the separation can be easily done approximately 1 m from the slave laser.

Figure 8.4 shows a sketch of the outgoing light as seen for example with the IR-viewer on a screen when the lens is displaced by 1.5 mm. This shift corresponds to a separation of about 15 mm between the master laser beam and the front reflection after 1 m of free beam propagation. This setup leads to an input angle of approximately 17° for the injected light at the diode's front facet. Naturally, one has to look separately at the incoming master beam because blocking it results in the disappearance of all other beams but the slave.

There are three observable spots in Fig. 8.4 that are not due to the beams of the master or slave lasers. The first spot left of the outgoing slave light in Fig. 8.4 can be identified as a reflection from the front facet or housing of the broad-area diode because it does not vanish even when the slave laser is turned off and it does not brighten when the driving current is turned up. Approximately 10% of the master laser's intensity entering the lens system in front of the slave is reflected back into the beam, producing this spot. This number is extremely stable and hardly changes with any of the parameters discussed here or in the following sections. This result naturally means that the reflectivity of the front part of our broad-area diode is, in contrast to many other diode lasers, not extremely low. Fresnel's law for a beam hitting a front facet made of GaAlAs at normal incidence predicts a reflectivity of roughly 30%. Therefore the diode's anti-reflection coating reduces it only by a factor of three. That in turn means that the gain inside the diode, according to the

discussion following Equation (2.4) is only approximately 10, while the gain would be about 100 for a reflectivity of 1%. This sets severe restrictions on the diode's usefulness for multi-pass amplification as discussed below and in chapter 9.

The other two spots in Fig. 8.4 correspond to beams shown in Fig. 4.1 as output beams, i.e., they are the result of amplification and prove that it is in principle possible to obtain clearly separated light in one longitudinal mode. Their intensity increases with increasing driving current of the broad-area diode as expected. The very left spot contains only half the intensity of the other one and therefore probably corresponds to a beam partly absorbed at one edge of the active layer. Ray tracing the beam through the active layer actually shows that only two beams can be expected to be emitted by a 200 μm broad-stripe at such a large input angle.

The increase in intensity with driving current is quite smooth, so interference effects inside the active layer (as seen for small input angles and dominating the behavior in a Fabry-Perot cavity) are not important. This can be expected from our model for a large input angle because the beams are hardly overlapping at all. The intensity starts to rise well below the threshold current at 0.1 A to 0.2 A and more or less saturates at a driving current of 0.8 A. It is interesting that the amplified intensity slightly decreases near the maximum driving current. The increase with increasing master laser output is quite linear.

The drawback of using a large input angle is that the intensity contained in the amplified beams is low and it is impossible to increase the total

power (including the front reflection) above 30 mW, even at the highest input intensities. So the break even point is not even reached in this setup because the master laser produces 90 mW of single-mode power without any amplification. This low power is either due to the fact that the gain factor of our diode is indeed not high, as one might expect from the front reflection, or that we are not able to couple more than a tiny fraction of the master beam into the active area. Moreover, for large input angles, only a small fraction of the active layer is actually influenced by the injected light.

One way to circumvent the low gain in each round trip is to decrease the input angle and thus increase the number of emitted beams, as described in Section 4.2. However, the linear, smooth behavior changes drastically when the input angle is reduced. At angles near 0°, the active layer actually operates as a two-dimensional cavity as discussed in Section 4.2, because the light is reflected back and forth several times. Because many beams overlap inside the active layer, constructive or destructive interference between the beams dominates the amplification behavior. Therefore, features like the cavity length and the injected wavelength, which are unimportant for large input angles, are as important as in a Fabry-Perot cavity (see Section 6.3) because only constructive interference inside the cavity and in the output beam lead to efficient amplification. In general, the efficiency of the amplification can be much higher for small input angles than for large ones because the light makes more passes through the active medium. However, the whole system is more sensitive to different parameters that change the ratio of the effective cavity length to the input wavelength such that it becomes unstable. This effect is discussed in Section 8.3 along with the effects of driving current and

temperature changes, i.e., the parameters that reveal the cavity-like behavior.

Furthermore, at small angles the different beams leaving the cavity are no longer distinguishable even by increasing the free propagation path further and further, because their divergence is larger than their separation angle. We have never observed a third amplified beam that would appear on the left of Fig. 8.4 before the beams merge into a single spot as the shift of the cylindrical lens is decreased. Since the output light consists of several interfering beams, it is questionable whether the resulting spot has the required spatially single-mode structure (see Chapter 9).

An even bigger problem at small angles is that the separation of the beams becomes small compared with the broad, free-running beam of the slave laser, and the whole structure shown in Fig. 8.4 lies inside the slave laser spot. This is mainly due to the fact that we are not able to reduce the divergence of the slave laser to less than 0.1°, even by using both the spherical 5 mm focal length and the cylindrical 200 mm focal length lens. Therefore, it is impossible to separate the amplified beam from the light emitted by the remaining slave laser free-running beam by just inserting a small pick-off mirror such that only the amplified beam is reflected. Here, measurements of the power in the amplified part of the light by a simple power meter are no longer useful. We measure the power by the height of the peak in the Fabry-Perot spectrum corresponding to the injected frequency. The cavity can be calibrated by measuring the power in the reflection of the master beam from the front surface of the slave laser while the slave is turned off because this is still a quantity measurable with a power meter. Fortunately, the amplified

beam does not spread in the same way such that picking up its intensity using a mirror is still possible without blocking the master. In a working multi-pass amplification system the amplified light must be spatially filtered to guarantee a clean single-mode structure. In this case the free-running slave laser light would be filtered out, and the overlap with the amplified light is not a real problem. It is only at nearly normal incidence that the pick up must be done with a beam splitter.

8.3 Driving Currents and Slave Temperature

Whenever the input angle is reduced to below 1°, the driving currents of both lasers and also the slave temperature become important parameters. We do not change the temperature of the master laser in order to keep its wavelength as stable as possible. At small input angles, according to the model introduced in Section 4.2, many beams overlap inside the active area and interference effects begin to be important, as in a Fabry-Perot cavity. Therefore the change of the cavity length by extremely small amounts should have a large impact on the actual amplified signal, i.e., the intensity in the injected mode of the outgoing beam (see also Section 8.2). Both driving current and temperature changes are known to cause such a variation in the cavity length.

Although our experiment is not sensitive enough to measure the cavity length directly, we verified rapid and periodic changes in the amplified intensity when we change these parameters (see the end of this section), as predicted by our saturated amplifier model and seen earlier, for example, in [6].

The measurements shown in Fig. 8.5 through 8.7 were taken at nearly

normal incidence (with the incoming master beam and front reflection overlapped, i.e., with no shift of the cylindrical lens) by inserting a beamsplitter with the master laser wavelength tuned to the cesium D_2-line. Figure 8.8 shows a measurement with the same setup but with the wavelength of the master laser shifted down in λ. At angles slightly larger than 0° but below 1°, the behavior of the system is similar. We only chose the beamsplitter alignment because this setup simplifies the measurement using the grating spectrometer. There were no realignments in between the measurements in each figure. Because the grating spectrometer's alignment is critical for the overall intensity scale, the measured intensities in different graphs are not necessarily comparable.

There are three different spectra (free-running slave, free-running master and amplified slave) plotted in each graph, in order to compare the free-running behavior of the two lasers directly with the spectrum where the slave laser is injected with light from the master laser. The free-running master-laser spectrum is taken using light from the front reflection. This procedure allows a comparison between the intensity in the front reflection and the intensity in the same mode due to the amplification process simply by comparing the heights of the two corresponding peaks.

The cleanest amplification occurs below and slightly above the threshold current of the broad area diode. As shown in Fig. 8.5, the free-running modes of the slave are completely suppressed and the spectrum is completely dominated by the injected light. Hence, the injected light decreases the population inversion in the active medium enough that free lasing is no longer

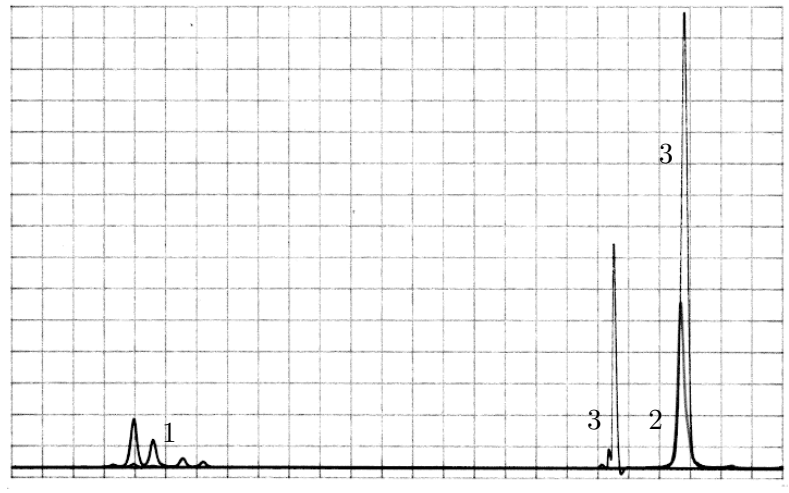

Figure 8.5: Spectra of the lasers: the slave laser is operated at 25 °C and its driving current is just above threshold (0.41 A). The master laser is driven with 151.8 mA. The free running slave lines (1) disappear completely in the spectrum where the master laser light is injected into the broad-area diode (3). The intensity in the reflection beam (2) is obviously increased due to injected light from the master laser. Furthermore, the injection of external light results in a side peak (3).

possible. In principle, this situation is ideal for multi-pass amplification. However, the intensity added to the amplified mode cannot be larger than the free-running output of the broad area diode, which at low driving current is itself low. Therefore, only 25 mW (including the front reflection, see Fig. 8.5) can be produced in this regime. This effect of completely dominating the free-running modes of the slave is relatively independent of the wavelength difference between the free-running and the injected light. We do not see it change even down to a free-running slave wavelength 10 nm below the master laser wavelength.

Generally, the overall change of the slave's free-running wavelength

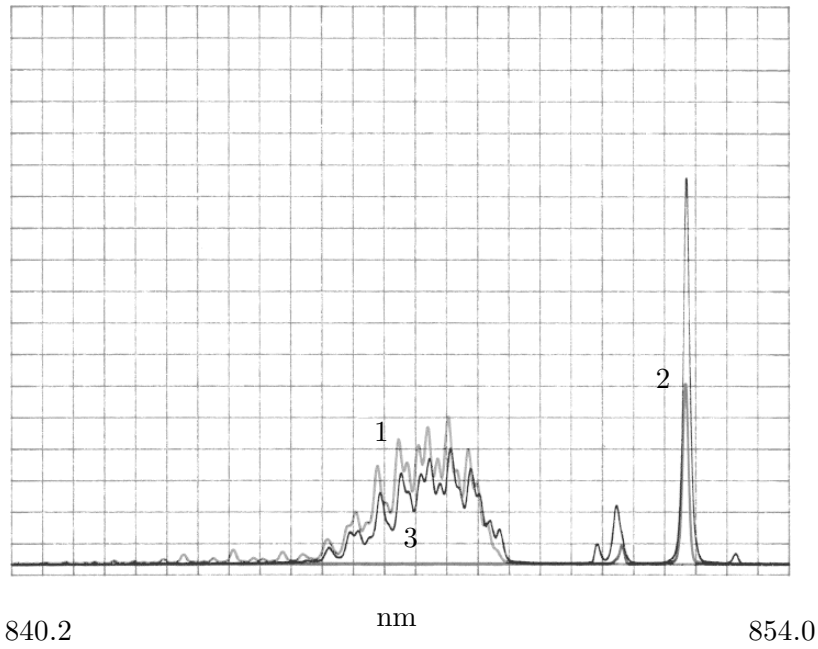

Figure 8.6: Spectra at 35 °C and 1.5 A driving current: the master laser is driven with 151.8 mA. Here, the free-running slave lines (1) are decreased due to the injection of master laser light into the slave laser's active layer (3), but far from being suppressed completely. The intensity in the injected mode (2) is approximately doubled. Here also, little side peaks are generated by the light injection.

with driving current and/or temperature does not play a dominant role in the overall amplification behavior. We do not observe any effect corresponding to the overall difference between the free running and injected wavelength. If there is anything changing, it is completely obscured in the effects discussed below. This behavior suggests that one might want to run the slave laser far away from the 852 nm line and then use a grating to separate out the amplified beam.

As soon as free lasing of the slave occurs at approximately 2-5% above its normal threshold current, the interference effects within the active medium

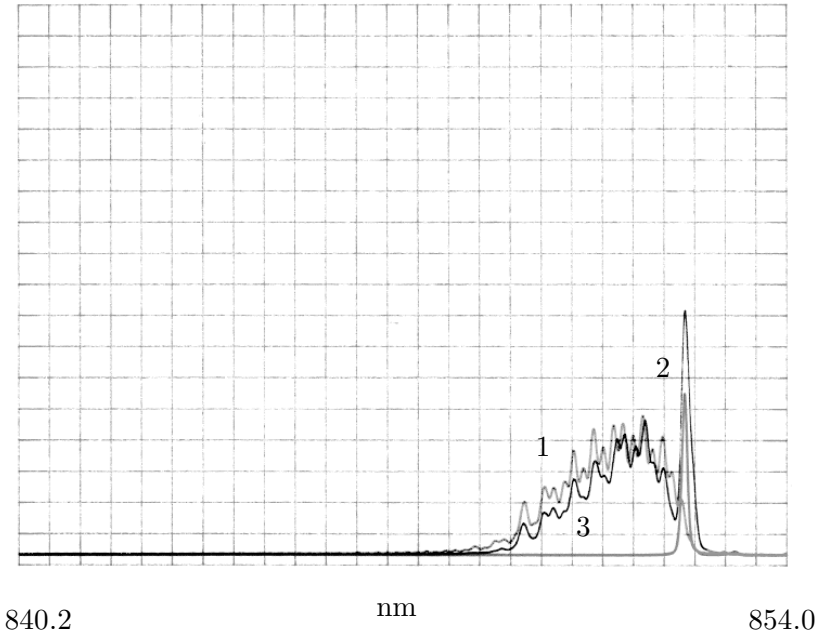

Figure 8.7: Spectra at 45 °C and 2.0 A driving current: the master laser is driven with 151.8 mA. The free running slave lines (1) are also decreased due to the injection of external light (3). Although here the spectra of the free running slave and the master almost overlap, the intensity in the injected mode (2) is hardly increased at all.

cavity become clearly visible. The intensity in the amplified mode changes rapidly with the driving current of both the slave and the master laser and also with the slave temperature. For example, increasing the driving current of the slave from threshold to its maximum value results in three to four cycles of increasing and decreasing intensity in the amplified beam, depending on the slave temperature and master laser driving current. These parameters shift the location of the peaks, because all three parameters together determine the ratio between the injected wavelength and the cavity length (or, more precisely the optical path length of one round trip).

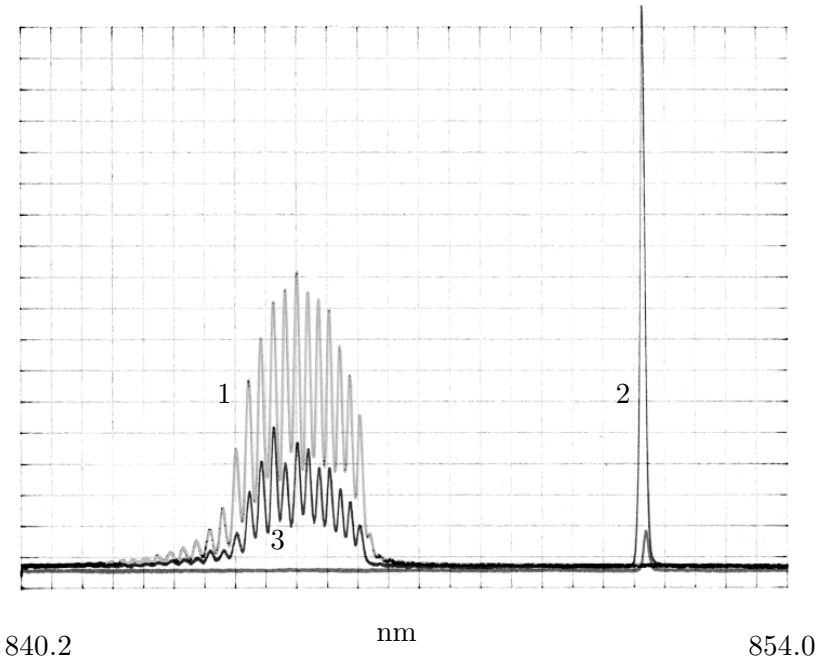

Figure 8.8: Spectra at 25 °C and 1.0 A driving current: the master laser is driven with 170.0 mA. The free running slave lines (1) are clearly suppressed due to the injection of light from the master laser (3). The intensity in the injected mode (2) is approximately 150 mW. This measurement corresponds to the highest value we have observed.

As usual for optical cavities, the peaks are very pronounced and narrow (see Section 6.3, especially Equation (6.4)). Setting the driving currents or the temperature to only slightly different values results in a rapid decrease in amplified intensity.

The minimum intensity during these oscillations is only slightly higher than the intensity in the front reflection. This means that essentially no intensity is coupled into the active layer (see Section 8.1 for details on the coupling). Figures 8.6 and 8.7 show graphs at more or less randomly chosen parameter values. The difference in efficiency of the amplification process is clearly visi-

ble. The cavity-like effects lead to the counterintuitive result that the intensity in the amplified beam is not necessarily highest at the highest slave driving current.

At certain parameter settings peaks in the spectra show up which are not present in either the master or slave free-running spectra. The origin of these side bands of the injected mode is not clear.

The parameter space can be most easily investigated by watching the *in situ* spectrum taken by the Fabry-Perot cavity. Figure 8.8 shows the spectra at parameters where the amplification is particularly effective. Here, the master wavelength is reduced to 846 nm, but this setting is not important. We find peaks of the same intensity at different parameter settings using the Fabry-Perot cavity as primary measurement instrument. Due to those measurements we are confident that we can reach 150 mW in the same longitudinal mode as the injected light. We are not able to make any conclusions about the spatial structure, therefore we do not know how much light is really contained in one spatial mode. This observation of 150 mW means that the break-even point of 90 mW can be easily achieved. For a discussion of the stability of the amplification efficiency, see Section 8.5.

As mentioned before, the Fabry-Perot cavity is not useful for gaining information about the remaining free-running modes of the slave laser, but the grating spectrometer spectra show that the intensity is more or less homogeneously lowered in each mode, corresponding to the efficiency of the amplification process.

8.4 Polarization

Since stimulated emission in the active layer is restricted to the vertical direction (in our alignment) only the part of the injected intensity polarized in this way is useful. Our experiment verifies this expectation. Varying the direction of polarization by turning the appropriate half-wave plate has no effect other than reducing the intensity in the injected mode according to the reduction of intensity in the vertically polarized component of the input intensity.

8.5 Dynamical Behavior

Most of the dynamical behavior we observe in our experiment is not directly related to the multi-pass amplification itself, but due to disruptions of the optical system. The largest effect is due to mode hopping of the master laser, which disturbs the experiment from time to time. It leads to sudden changes in the amplification behavior at small input angles, because the ratio of input wavelength to cavity length in the slave also hops to a different value. Other long time drifts (e.g., in the translation stages) yield in general a decreasing efficiency of the amplification when an optimal parameter configuration is chosen to start with. Finally, we also observe a time dependence in the amplification that we do not understand. Whenever the injected light is turned on, the amplification of the light as seen, for example, with the Fabry-Perot cavity is delayed by roughly one second. This effect is definitely not due to the turn-on of the master laser, because even blocking the master laser beam for a short time is enough to produce this effect. Even blocking it for periods shorter than one second results in the same effect. We do not have a satisfying

explanation for this effect.

Chapter 9

Conclusions

This thesis presents a detailed picture of our diode's multi-pass amplification behavior. We demonstrate the possibility of multi-pass amplification and show that the power in the amplified beam exceeds the input power of our master laser. Of course, we cannot claim that our observations can be generalized to other broad-area laser diodes. Nevertheless, the model for multi-pass amplification introduced in Section 4.2 is quite consistent with our experimental data. In particular, the cavity-like behavior of the diode at small input angles that vanishes for larger angles supports the validity of the model for our experimental setup. We hope that our theoretical introduction to diode lasers and theory of beam propagation will be a helpful reference for further work on multi-pass amplification.

Concerning our original goal of constructing a high-power single-mode laser system for experiments an cold cesium atoms, our project has to be considered incomplete. We have not been able to come even close to an amplified output power sufficient to make our setup an interesting alternative to other available lasers.

There are two possible reasons for the low efficiency of our broad area

laser diode. First, the critical small width of the active layer leads to the question if our alignment is appropriate for coupling a sufficient part of the master light in. In particular, we have not been able to try active mode matching because we have not had the necessary equipment at hand (e.g., a wide selection of aspherical lenses) and our ability to monitor the mode matching is limited. Solving these obvious problems could make a more effective injection locking of our diode possible.

The second reason for the limited success of our project might be the diode itself, in particular its antireflection coating. Our theoretical model and experimental experiences of other groups support the fact that a good anti-reflection coating of the diode's front facet is crucial for a good multi-pass amplification performance. The front reflection seen in our experiment even for small incident angles and the extreme cavity like behavior of our diode suggest that the diode does not have a sufficient anti-reflection coating. Our experimental data shows that the multi-pass amplification setup with the components described in Chapter 7 operates far from the ideal double-passed amplifier scheme. Furthermore, multi-pass amplification systems including a variety of broad-area diodes are now commercially available but none of them use our type of broad-area diode.

Although we have not reached our ultimate goal of engineering a working laser system, we have discovered a lot of interesting physics. We hope that our investigation of the free-running behavior of diode lasers, the validity of the presented multi-pass amplification model, and the dependence of amplification on different parameters will be helpful for further work on this

subject.

Appendices

Appendix A

Mathematica Programs

The Mathematica® code is typeset so as to distinguish it from the comments.

A.1 Ray Tracing

Generation of the matrices for different optical components:

`p[x_]:=1,x,0,1`

Free propagation along a path of length `x` in the chosen units

`l[x_]:=1,0,-1/x,1`

Lens of focal length `x` in the chosen units

`s[x_]:=x`

Shift away from the optical axis when components are not centered

The setup for which calculations are to be done is simply implemented by listing the components including shifts and free propagation. If a component is shifted this shift has to be included in the list again in the opposite direction after the component. The default setting here is no setup at all (`p[0]`).

`list:=p[0]`

The `compute` function is used in the `do`-function to calculate the matrix describing the setup from the list of components in a simple loop.

```
compute[comp_]:=compute[comp]=Block[x=comp,y=1,0,0,1,
                For[i=1,i<Length[x]+1,i++,y=x[[i]].y];
                Return[y]]
```

The do-function finally calculates the final position and slope of the beam after the propagation through the setup from the initial conditions. The `initial` variable has to be a two component list out of initial position and initial slope.

```
do[initial_,list_]:=Block[in=initial,inlist=list,actual=p[0],
                For[i=1,i<Length[inlist]+1,i++,
                If[Length[inlist[[i]]]==2,
                     actual=Join[actual,inlist[[i]]],
                     in=compute[actual].in;
                     in[[1]]=in[[1]]+inlist[[i]][[1]][[1]];
                     actual=p[0]]];
                Return[compute[actual].in]]
```

A.2 Gaussian Beams

An abbreviation for the Mathematica symbol `Infinity` is defined as

```
inf:=Infinity
```

Again the matrices for free propagation and lenses are implemented by

```
p[x_]:=1,x,0,1
l[x_]:=1,0,-1/x,1
```

The setup is also implemented like in Appendix 3.1. No shifts of optical components are possible.

```
list:=p[0]
```

The used wavelength is set. The default setting is 852×10^{-9} m

```
lambda:=852*10^(-9)
```

The `beginning` function is used in `do` and `dodiv` and converts the initial beam parameters in a form useful for these functions

```
beginning[R_,om_]:=1/(1/R-I*lambda/(Pi*om*om))
```

Same function like in Appendix 3.1

```
compute[comp_]:=compute[comp]=Block[x=comp,y=1,0,0,1,
                For[i=1,i<Length[x]+1,i++,y=x[[i]].y];
                Return[y]]
```

The `do`-function calculates the beam radius after a certain setup implemented in list from the initial beam radius `R` and the inverse divergence, e.g. `in=inf` means no initial divergence.

```
do[R_,in_,list_]:=Sqrt[Abs[-lambda/(Im[1/((beginning[R,in]
                * compute[list][[1,1]] + compute[list][[1,2]])
                /(beginning[R,in] * compute[list][[2,1]]
                + compute[list][[2,2]]))]*Pi)]]
```

The `dodiv`-function is in principle the same as the `do`-function but calculates the final divergence of a beam.

```
dodiv[R_,in_,list_]:=Re[1/((beginning[R,in]*compute[list][[1,1]]
                + compute[list][[1,2]])/(beginning[R,in]
                * compute[list][[2,1]] + compute[list][[2,2]]))]
```

Appendix B

Conversion of Resistance into Temperature

For thermal resistors (also called termistors) there is a simple equation for converting temperature into resistance namely the Steinhart-Hart Equation reading:

$$\frac{1}{T} = A + B \ln R + C(\ln R)^3 \tag{B.1}$$

where A, B and C are constants depending on the used termistor, R is the resistance and T is the temperature in Kelvin. In our case the values for the constants are

$$\begin{aligned} A &= 0.00269158 \\ B &= 0.000285179 \\ C &= 4.73608 \times 10^{-7} \end{aligned} \tag{B.2}$$

and one gets Tab. B.1 for a temperature ranging from 0 to 50 degrees Celsius.

T ($^\circ C$)	R (kΩ)	T ($^\circ C$)	R (kΩ)	T ($^\circ C$)	R (kΩ)
0	28.15	17	13.70	34	7.140
1	26.92	18	13.16	35	6.885
2	25.76	19	12.64	36	6.641
3	24.65	20	12.15	37	6.406
4	23.60	21	11.68	38	6.181
5	22.60	22	11.23	39	5.965
6	21.64	23	10.80	40	5.758
7	20.74	24	10.39	41	5.559
8	19.87	25	10.00	42	5.369
9	19.05	26	9.624	43	5.186
10	18.26	27	9.265	44	5.010
11	17.51	28	8.921	45	4.841
12	16.80	29	8.591	46	4.678
13	16.12	30	8.276	47	4.522
14	15.47	31	7.973	48	4.372
15	14.85	32	7.684	49	4.228
16	14.26	33	7.406	50	4.089

Table B.1: Conversion of resistance into temperature for the used NTC-resistor

Bibliography

[1] G.L. Abbas, S. Yang, V. Chan, and J. Fujimoto, *Opt. Lett.* **12**, 605 (1987).

[2] G.L. Abbas, S. Yang, V. Chan, and J. Fujimoto, *J. Quant. Opt.* **24**, 609 (1988).

[3] L. Goldberg and M.K. Chun, *Appl. Phys. Lett.* **53**, 1900 (1988).

[4] S.Q. Shang and H. Metcalf, *Appl. Opt.* **28**, 1618 (1989).

[5] W. Nagengast and K. Rith, *Opt. Lett.* **22**, 1250 (1997).

[6] A.C. Fey-den Boer, H.C.W. Beijerinck, and K.A.H. van Leeuwen, *Appl. Phys. B* **64**, 415 (1997).

[7] M. Praeger, V. Vuletic, T. Fischer, T. Haensch, and C. Zimmermann, *Applied Physics B* **67**, 163 (1998).

[8] P.W. Milonni and J.H. Eberly, *Lasers* (Wiley Interscience, New York, 1988).

[9] W. Demtröder *Experimentalphysik 3*, ch. 8, 1. Auflage (Springer, Berlin, 1996).

[10] H. Eichler and H.J. Eichler, *Laser (Grundlagen, Systeme, Anwendungen)*, 2. Auflage (Springer, Berlin, 1991).

[11] F.K. Kneubühl and M.W. Sigrist, *Laser*, 2. Auflage (Teubner, Stuttgart, 1989).

[12] N.W. Ashcroft and N.D. Mermin, *Solid State Physics* (W.B. Saunders Company, Philadelphia, 1976).

[13] A. Yariv, *Quantum Electronics*, ch. 11 (John Wiley and Sons, New York, 1988).

[14] J.T. Verdeyen, *Laser electronics*, 3rd ed. (Prentice Hall, Englewood Cliffs, 1995).

[15] A.E. Siegmann, *Lasers* (University Science Books, Mill Valley, 1986).

[16] H. Adachihara, O. Hess, E. Abraham, P. Ru, and J.V. Moloney, *J. Opt. Soc. Am.* **10**, 658 (1993).

[17] E. Hecht, *Optics*, 3rd ed. (Addison Wesley Longman, New York, 1998).

[18] C. Gerthsen, H.O. Kneser, and H. Vogel, *Physik*, 16. Auflage (Springer, Berlin, 1989).

[19] W. Demtröder, *Laser Spectroscopy*, 2nd ed. (Springer, Berlin, 1996).

[20] P.A. Tipler, *Physics*, 2nd ed. (Worth Publishers, New York, 1982).

[21] K.B. MacAdam, A. Steinbach, and C. Wieman, *Am. J. Phys.* **60**, 1098 (1992).

Vita

Nicole Helbig was born on July 12, 1976 in Potsdam, Germany as the daughter of Jürgen Helbig and Sabine Helbig. She received her Abitur from the Rudolf-Diesel-Gymnasium in Augburg in 1995 and began studying physics at the Universität Würzburg in November of the same year. After receiving her Vordiplom in August 1997 and studying physics for one additional year in Würzburg, she entered the graduate school of the University of Texas at Austin in August 1998.

Permanent address: Peter-Henlein-Straße 7
97688 Bad Kissingen
Germany

This thesis was typeset with LaTeX[‡] by the author.

[‡]LaTeX is a document preparation system developed by Leslie Lamport as a special version of Donald Knuth's TeX Program.